catalysts

MDPI

Review

Intensification of Photo-Assisted Advanced Oxidation Processes for Water Treatment: A Critical Review

Jorge Rodríguez-Chueca [1], Jaime Carbajo [2,*] and Patricia García-Muñoz [1]

[1] Department of Industrial Chemical & Environmental Engineering, Escuela Técnica Superior de Ingenieros Industriales, Universidad Politécnica de Madrid, Calle José Gutiérrez Abascal 2, 28006 Madrid, Spain
[2] Chemical and Materials Engineering Department, Universidad Complutense de Madrid, Pl. de las Ciencias, 2, 28040 Madrid, Spain
* Correspondence: jaime.carbajo@ucm.es

Abstract: In recent decades, ultraviolet-assisted advanced oxidation processes (UV-AOPs) have been successfully applied to remove a wide range of contaminants from polluted water. Despite this, their extended use on an industrial scale is still far from being a reality, largely limited by the operational costs that these processes still entail. In recent years, many researchers have been working to increase UV-AOP efficiency and reduce capital and operating costs. This work aims to review different strategies devoted to the intensification of UV-AOPs. Firstly, the optimization of operational parameters, such as catalyst loading, pH, temperature, or oxidant concentration, has been reviewed as a strategy to augment the efficiency of the photocatalytic processes and reduce reagent consumption and/or treatment time. The review also discusses the development of photocatalytic materials to intensify the UV-AOPs process, and finally, the combination or integration of different UV-AOPs for the treatment of pollutants is also examined.

Keywords: intensification processes; advanced oxidation processes; UV assisted; water treatment; contaminants of emerging concern

check for updates

Citation: Rodríguez-Chueca, J.; Carbajo, J.; García-Muñoz, P. Intensification of Photo-Assisted Advanced Oxidation Processes for Water Treatment: A Critical Review. *Catalysts* **2023**, *13*, 401. https://doi.org/10.3390/catal13020401

Academic Editor: Aurora Santos

Received: 29 December 2022
Revised: 3 February 2023
Accepted: 8 February 2023
Published: 13 February 2023

1. Introduction

In recent decades, sustained and ubiquitous emission of persistent organic pollutants (i.e., pharmaceuticals, pesticides, personal hygiene products, among others) into the environment has triggered the demand for more efficient wastewater treatment technologies. In this regard, advanced oxidation processes (AOPs) have emerged as promising alternatives to conventional treatments [1]. The advantages of these processes include rapid and non-selective reactions of $HO^{\bullet}$ with pollutants, the capability of hydroxyl radicals to mineralise organic pollutants into stable inorganic compounds such as water, carbon dioxide and salts, and mild operating conditions. Furthermore, when AOPs are assisted or mediated by UV light (UV-AOPs), the ability to treat persistent pollutants or provide efficient disinfection is enhanced by increasing the efficacy of oxidant agents (H_2O_2, $S_2O_8^{2-}$, O_3, etc.) conversion into active free radicals ($HO^{\bullet}$, $SO_4^{\bullet-}$).

There is a wide spectrum of UV-AOPs treatments which may be classified as homogeneous or heterogeneous, as shown in Figure 1. Photo-assisted homogeneous or heterogeneous Fenton ($H_2O_2/Fe^{2+}/UV$) uses UV–Vis irradiation for the photolysis of Fe^{3+} complexes by regenerating Fe^{2+}, which subsequently decompose H_2O_2 into active $HO^{\bullet}$. In heterogeneous photocatalysis (TiO_2/UV), the absorption of a photon with energy equal to or higher than the band-gap of the semiconductor leads to the formation of electron–hole pairs (e^-/h^+) and subsequently to hydroxyl radicals. For their part, O_3- or H_2O_2-based AOPs can also be combined with UV to form active hydroxyl radicals (O_3/UV; $O_3/H_2O_2/UV$ or H_2O_2/UV). In addition, UV-AOPs can use sulfate radicals ($SO_4^{\bullet-}$) as powerful oxidants with a high redox potential of 2.6 V (approximate to $HO^{\bullet}$ (2.8 V)) [2] by activating potassium/sodium persulfate (PS) or potassium peroxymonosulfate (PMS) salts.

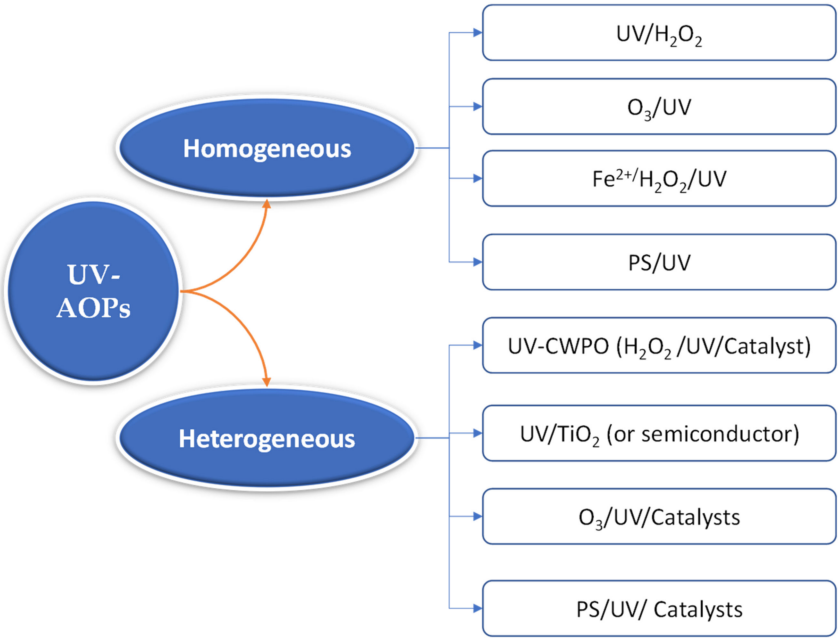

Figure 1. UV-AOPs classification.

Despite the undeniable advantages of UV-AOPs already described, there are significant limitations to the implementation of these processes on an industrial scale. Perhaps, the latter may be explained by the relatively high operating costs (light energy, chemical reagent consumption, etc.) and capital costs (photo-reactors design complexity, even when solar light is employed). Other specific limitations may also be cited, such as optimisation requirements of oxidant dosage to avoid excessive $HO^{\bullet}$ formation, the acidic conditions and iron removal requirements in photo-Fenton processes, or design photoreactor limitations, as UV light penetration is strongly attenuated by turbidity [3]. Therefore, full-scale UV-AOPs application is very limited, and their implementation is still far from being a reality [4,5].

In this context, intensification of UV-AOPs (i.e., setting innovative improvements in the process to increase efficiency or lower capital and operating costs [6]) is undoubtedly a promising avenue to improve the feasibility of these processes on an industrial scale. In recent years, many researchers have been working to increase the efficiency of UV-AOPs and reduce capital and operating costs. Nevertheless, currently, very few review works address effective strategies for improving or intensifying AOPs processes, and to the best of our knowledge, none of these reviews focus specifically on UV-assisted AOPs. Therefore, this review attempts to compile some of the main strategies that can be implemented to optimise UV-AOPs, including the optimisation of operation conditions, the employment of novel and bi-functional catalysts, and the synergistic combination of UV-AOPs.

One strategy to intensify the efficiency of UV-AOPs processes is to optimise operating conditions to reduce reagent consumption and minimise the time needed for pollutant removal and mineralisation. The efficiency of these processes is affected by different operational parameters such as catalyst loading, pH, temperature, and oxidant concentration. Many recent studies have focused on optimising these parameters to intensify the photocatalytic process. In the case of catalyst loading, increasing it can improve the pollutant removal rates, but exceeding the maximum optimal value can slow the rate of mineralisation. Different studies have found varying optimal concentrations for different catalysts and conditions, and some have developed models to better understand the dependence of reaction rates on catalyst loadings.

Another section is focused on the use of bifunctional catalysts used for the photocatalytic treatment of polluted water as a strategy for the process intensification. In recent years, much effort has been spent for developing photocatalytic materials to improve the process efficiency. This intensification has mainly been conducted in two directions: to

reduce physical limitations of the reaction and to increase the overall yield of the treatment, which is also related to chemical limitations. The main approaches to augment the overall yield via photocatalysts can be divided into two main categories: design orientated to reduce mass and photon transfer limitations, and design of bifunctional catalysts that increase the generation of oxidising species. These latest, which are bifunctional catalysts, play a dual role in the process. A bifunctional catalyst can be considered for every non-consumed material with a double role in the reaction, i.e., bulk semiconductor nature and with surface catalytic sites, or the combination of a high adsorption and a photocatalytic role. These strategies are further discussed, including the main approaches found in the literature for each of them.

Finally, this review discusses the combination of different photo-assisted UV-AOPs, for the treatment of pollutants as intensification strategy. The combination of processes is often carried out with the aim of obtaining a positive synergistic effect [7], but this is not always the case, and antagonistic effects could be observed [8]. The text describes hybrid (or single-step combined process) and sequential (or two-step combined process) systems that combine AOPs with other technologies, for instance with other AOPs or with other kind of technologies (i.e., physical, chemical or biological). The combination of processes is often associated with a further step in the maturity of the technology and its proximity to application on a larger scale. It is for this reason that, throughout this section, a greater number of close-to-reality works using pilot scales are observed. However, more research is needed to understand the mechanisms of these combinations and to improve their applicability and efficiency at larger scales.

2. Intensification of Operational Conditions in UV-AOPs

Among all intensification strategies, probably one of the most obvious and effective is the optimization of operating conditions that aim to either reduce reagent consumption or minimize the time required to achieve the appropriate pollutant removal and/or mineralization. This section specifically covers recent approaches devoted to the optimisation of the most relevant operational conditions. In this regard, the efficiency of the UV-AOPs processes is severally affected by different operational parameters such as catalyst loading, pH, temperature and or oxidant concentration, among others [9]. In this section, we focus on those variables that can be intensified in operation, leaving aside those that are given by the nature of the effluent to be treated (pollutant load, presence of salts) or by the reaction system (reactor configuration, nature, and intensity of the irradiation). Many works have addressed new strategies for optimising these parameters in recent years to intensify the photocatalytic process, some of which are listed in Tables 1–4. Furthermore, Figure 2 shows the key points to be considered for the optimisation of operating conditions in UV-AOPs.

2.1. Catalyst Loading

In catalytic processes, the increase in catalyst loading usually boosts the formation of active radicals, which is translated into higher pollutant depletion rates. Nevertheless, the catalyst load can only increase up to a certain maximum value in ultraviolet (UV) catalytic processes. Exceeding this optimum results in a shielding phenomenon in which a large part of incident radiation is reflected by scattering, preventing most photons from reaching the catalyst particles, causing the rate of mineralisation to slow down [10].

In UV-TiO_2 processes, the optimum catalyst mass has usually been empirically fixed. In this regard, many works have optimised catalyst concentration for different reactor geometries and applications such as dyes (methylene blue) [11,12], emerging pollutants (caffeine) [13], pharmaceuticals (diclofenac, cefotaxime, ibuprofen) [14–16] or pesticides [17], among others. Similarly, optimal catalyst loadings have also been observed in other UV-activated heterogeneous catalytic systems, such as UV light-assisted persulfate activation by Cu^0-Cu_2O for the degradation of sulfamerazine [18] or persulfate activation by polymeric photocatalysts based on g-C_3N_4 [19]. As can be seen in Table 1, the optimum concentrations vary greatly (0.3 g/L to 2.5 g/L) depending on incident irradiation, path length, and type

of catalyst. Optimal loading changes completely with different types of catalysts, such as TiO_2 and ZnO, under the same conditions [15].

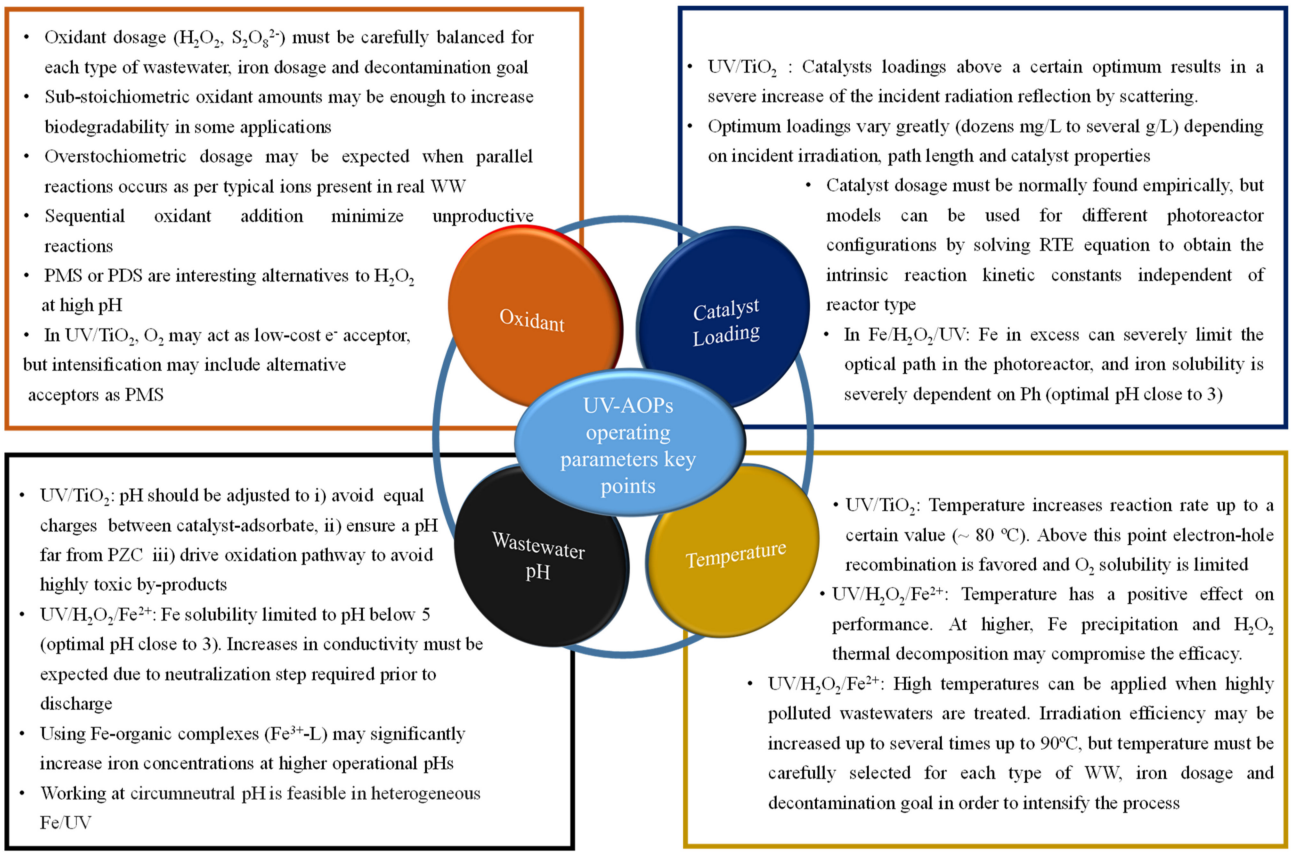

Figure 2. Key aspects for the optimisation of operating conditions in UV-AOPs.

Finding the optimal concentration for each photocatalytic system is not a practical strategy for engineering purposes in the design and optimisation of large-scale photocatalytic reactors [20]. For this reason, some works have focused their efforts on the description of a model including, in an explicit way, the dependence of the reaction rate on the volumetric rate of photon absorption in catalyst suspensions. Therefore, Carbajo and Tolosana et al. [21,22] used reflectance measurements to obtain the extinction coefficients in the UV-A range and the radiation profiles inside the photoreactor to solve the radiative transfer equation (RTE). The corresponding kinetic parameters were well suited to optimise catalyst loadings for different morphological and hydrodynamic characteristics such as titanium dioxides P25, P25/20, and P90, which represents a significant step forward in the design and optimisation of large-scale photocatalytic reactors. For their part, Casado et al. [20] radiated TiO_2 suspensions with concentrations between 0.005 and 5 $g \cdot L^{-1}$ to develop a model considering both computational fluid dynamics (CFD) and the resolution of the RTE. This approach includes not only the effect of fluid mechanics, mass transport and chemical reaction, but also radiation transfer, showing an optimum catalyst loading around 0.1–0.2 $g \cdot L^{-1}$. Li puma and co-workers [23,24] studied the radiative transfer phenomena in different reactor configurations (solar annular and rectangular channel flat reactors), by coupling a six-flux radiation absorption-scattering model to the Henyey–Greenstein scattering phase function (SFM-HG). The authors provide a new approach to measure the impact of catalyst loading and optical properties suspensions of two different photocatalysts as TiO_2 (or modified Ag-TiO_2) and goethite.

In UV/Fe/H_2O_2 processes, the amount of Fe also plays a crucial role in the production of active radicals. For example, a few mg/L of iron may be enough for the treatment of low concentrated wastewater containing emerging pollutants such as carbamazepine or

5-Fluorouracil [25,26], but catalyst loading could require up to hundreds of mg/L Fe when treating sour water from a refinery plant [27]. Although, generally speaking, increases in iron concentration always led to increases in disappearance kinetic rates, at a certain level, this improvement is residual and the efficiency decreases significantly due to the ineffective decomposition of H_2O_2 caused by excess iron, which can act as a scavenger of hydroxyl radicals, reducing process efficiency (see Equation (1)):

$$Fe^{2+} + HO^{\bullet} \rightarrow OH^{-} + Fe^{3+} \quad (1)$$

Furthermore, excess Fe can severely limit the optical path in the photoreactor [9], reducing the efficiency of photon absorption inside the photoreactor. The influence of iron and irradiance level on pyrimethanil degradation by the photo-Fenton process was analysed by Cabrera Reina et al. [28]. The authors realised that the efficacy of the treatment clearly improved by increasing the dose of Fe from 8 to 20 mg·L^{-1}; thus, iron was no longer the rate limiting factor as the process improves with irradiance, but another increase to 32 mg·L^{-1} caused severely inefficient H_2O_2 consumption, and similar degradation rates were observed due to the undesirable excess of radical production. Under the conditions of this study, the lowest costs values were found with 20 mg·L^{-1} of Fe, proving the ineffectiveness of increasing Fe doses beyond a certain point. Therefore, in UV/Fe/H_2O_2, the Fe dosage must be specifically balanced with the amount of H_2O_2 and the type of wastewater.

Table 1. UV-AOPs intensification by catalyst loading optimisation.

Photocatalytical System	Target Pollutant	Catalysts Loading Conditions	Remarks	Experimental Remarks	Ref.
TiO_2/UV-A	Methylene Blue (Dye)	[catalyst] = 0.5, 1, 1.5 g/L	Optimum achieved at 1 g/L (k = 0.0801 min^{-1})	MB_0 = 60 mg/L; pH neutral; T = 20 °C, UV-A = 40 W/m^2 Immersion Reactor, Ø = 76 mm	[11]
TiO_2/Solar	Methylene Blue, Dichloroacetic acid, 4-Chlorophenol	[catalyst] = 0.2, 0.25, 0.3, 0.35 g/L.	Optimal photocatalyst loading 0.25 g/L. 99% MB degradation at 8000 J/m^2.	$[MB]_0$ = 10 ppm, flow rate = 24 L/min, pH = natural (7.45). Solar Pilot-scale Offset Multi Tubular Photoreactor (OMTP), Ø = 32 mm	[12]
1% Mg-ZnO-Al_2O_3/UV-A/B	Caffeine	[catalyst] = 0.1–1.5 g/L	Optimal photocatalyst loading 0.3 g/L (1% Mg-ZnO-Al_2O_3) Caffeine degradation was 98.9%	[Caffeine] = 20 mg/L. Cylindrical Pyrex immersion photoreactor (2 L). UV Hg lamp (400 W). T = 25 °C	[13]
TiO_2/UV-A	Diclofenac (DIC)	[catalyst] = 0.1–2 g/L	k_{app}, (0.35 min^{-1}) was optimal at a mass of catalyst of 1.0 g/L	$[DIC]_0$ = 8 mg/L. T = 293 K, pH = 6. 800 mL glass immersion photoreactor (Ø = 7.5 cm) TQ 150 mp Hg lamp (λexc < 366 nm)	[16]
TiO_2/UV ZnO/UV	Cefotaxime	[catalyst] = 1.0–2.5 g/L	≈84.2% of Cefotaxime removal optimized at 2.3 g/L of TiO_2 and around 1.45 g L^{-1} of ZnO.	Sunlight sim. Xe lamp (300–800 nm) 250 W/m^2 [Cefotaxime] = 20 mg/L, T = 35 °C	[15]
TiO_2/UV-LED	Ibuprofen (municipal and pharmaceutical spiked MWW)	[catalyst] = 0.5–4 g/L	100% removal of IBU and 55% removal of DOC. k_{app}, (0.024 min^{-1}) was optimal at 2.5 g/L	Lab-scale photoreactor: 10 W UVhigh LEDs (λ_{max} = 382 nm); V = 250 mL, IBUP (up to 213 mg/L)	[14]
$Na_2S_2O_8$/TiO_2/Solar	Mixture of 8 pesticides in agro-phitosanitary wastewater	[catalyst] = 100 to 500 mg/L	The degradation rate increases up to 300 mg/L of catalyst loading	[Pesticides]: 0.21 mg/L (hexythiazox) to 5.97 mg/L (thiamethoxam) CPC photoreactor, Ø 14.6 cm, V = 180 L (75 L illuminate V)	[17]

Table 1. *Cont.*

Photocatalytical System	Target Pollutant	Catalysts Loading Conditions	Remarks	Experimental Remarks	Ref.
PS/Cu^0-Cu_2O/UVA	sulfamerazine	[catalyst] = 0.06 to 1 g/L	SMZ removal increases to 0.2 g/L	$[SMZ]_0$ = 50 mg/L; $[PS]_0$ = 0.8 g/L, λ_{max} = 382 nm, initial; pH = 7, 25 °C; photo-reactor with Hg lamp (800 W)	[18]
g-C_3N_4/PMS/Vis system	Acid Orange 7 (AO7)	[catalyst] = 0.05 to 1.2 g/L	The degradation rate increased with catalyst load to 0.8 g/L	500 W xenon lamp, [PMS] = 0.4 g/L, [AO7] = 20 mg/L, T = 25 °C	[19]
UV/TiO_2	MeOH	Radiation field was simulated. [TiO_2] = 0.005–5 g/L	Maximum at 0.2 g/L Radiative model was confirmed with MeOH oxidation experiments	Differential photoreactor (ODPR). V = 3.2 mL, quartz cell (Hellma QS-130), optical path = 1 cm; 36 UV-A LEDs (365 nm, Rad flux = 410 mW at 700 mA)	[20]
P25, P25/20 and P90 (TiO_2)/UV	Phenol (Model)	Radiation field was simulated. [TiO_2] = 0.1–1.5 g/L	P25 and P90 optimum catalyst load (0.25–0.50 g/L) was 2 times P25/20 (∼0.7–1.0 g/L) The kinetic model was successfully validated by experimental data (phenol oxidation)	1L Pyrex slurry photoreactor (Ø = 76 mm), 15 W × 6 Black Light Blue lamps(15W) $[phenol]_0$ = 50 mg/L, pH_0 = 6.0, irradiance = 38.4 W/m^2	[21,22]
TiO_2, Ag-TiO_2, goethite/ UV–Vis	2-hydroxybenzoic acid (2-HBA)	Initial rate of photon absorption (IRPA) was correlated to optimum catalyst Concentration [TiO_2] = 0.1–2 g/L	The apparent optical thickness: τapp = 4.1–4.4 provides optimum catalyst and reactor performance. Intrinsic kinetic parameters of 2-HBA photocatalytic oxidation were determined.	Flat plane photo-reactor (thickness L = 1 cm) or annular reactor (Ø int = 0.054 m), cylindrical lamp mounted axially [2-HBA] = 0.2 mmol/dm^3; T = 22; pH = 4.0 UVA to natural light (UVA up to 89.4 W/m^2	[23,24]
Fe^{2+}/H_2O_2/ UV–Vis	5-fluorouracil	[Fe^{2+}] = 0–100 mg/L	Performance increased to a ferric ion concentration of 4.5 mg/L At higher concentrations, the degradation rate increases marginally	double-walled Pyrex glass reactor, thermostated in a solar with a xenon lamp (1.5 kW, 500 W/m^2) 100 mL of 5-FU solution (10 mg/L); pH = 3; H_2O_2 = 0–90 mg/L	[25]
Fe^{2+}/H_2O_2/ UV-B	Sourwater from petroleum refineries	[$FeSO_4$] = 0.13–0.4 g/L	DOC removal was optimised with the highest amount of iron.	2 reactors operating in continuous mode. Fenton (400 mL) and Photo-Fenton (1600 mL), with UV-B lamp (15 W) [COD] = 850–1020 mg/L; $[H_2O_2]_0$ = 4 g/L, $[FeSO_4]_0$ = 0.1–0.4 g/L.	[27]
Fe^{2+}/H_2O_2/UVA	pyrimethanil	[Fe^{2+}] = 8, 20 and 32 mg/L	At 20 mg/L, the treatment always improved with irradiance (process was photo-limited). At 32 mg/L, the excess of iron was counter-productive.	Lab-scale raceway photo-reactor in a SolarBox equipped with Xenon lamp (300–800 nm) [H_2O_2] = 35 mM, pH = 2.8	[28]

2.2. pH

In heterogeneous photocatalysis, pollutant–photocatalyst interactions are directly linked with the charge of photocatalyst particles, its state of aggregation, and the speciation of pollutants; thus, photocatalytical performance is governed by pH modifications. For example, the point of zero charge (PZC) in TiO_2 is usually in the range between 5.6 and 6.8 [29]; thus, when the pH is below the point of zero charge (pH < pHpzc), the catalytic surface is positively charged, while when the pH of the solution is higher (pH > pHpzc), the TiO_2 surface becomes negatively charged (Equations (2) and (3)):

$$\text{-Ti-OH} + H^+ \rightleftarrows \text{-TiOH}_2{}^+ \quad (2)$$

$$\text{-Ti-OH} + \text{OH-} \rightleftarrows \text{-TiO}^- + H_2O \quad (3)$$

Therefore, when possible, pH should be adjusted to: (i) avoid equal charges between catalyst and adsorbate, (ii) ensure a pH far from PZC, limiting particle aggregation, and (iii) drive the oxidation pathway to avoid highly toxic by-product formation. Many examples of these strategies are collected in Table 2. Seid and co-workers [30] studied the effect of pH in the treatment of several nitrosamines (nizatidine, trimebutine, and metoclopramide), finding that working at an initial pH $\geq$ 5.6 reduced by half the formation of carcinogenic nitrosamine by-products. For their part, Elhalil et al. [13] found that the photocatalytic degradation of caffeine using 1% Mg-ZnO-Al_2O_3 as the photocatalyst was significantly enhanced operating at pH above PZC, thus favouring the adsorption of the protonated caffeine molecule (pK_a = 10.4) onto the negatively charged catalyst surface. Similarly, the importance of PZC identification was revealed when different TiO_2 was tested during methylene blue degradation [31]; therefore, negatively charged TiO_2 surfaces with TiO_2 NP prepared at pH 7.0–10 clearly improved process efficacy favouring interaction with the cationic dye. Carbajo et al. [32] also analysed the effect of the chemical nature of different substrates on the degradation mechanism and observed that at pH 2.7, the interaction between titania catalysts (positively charged) and the dichloroacetate anion $CHCl_2COO^-$ (pK_a = 1.26) favoured DCA photodegradation by direct attack of photogenerated holes (h^+), while on the contrary, indirect attack OH appears to govern the removal of phenol (pK_a = 9.9) at natural pH.

UV/Fe/H_2O_2 systems should usually operate in a narrow pH range (2.8–3.0) to optimize $HO^\bullet$ production [33]. At higher pH, catalyst precipitation occurs as iron hydroxide, while the consumption of HO radicals by protons is enhanced at pH < 2.5 according to Equation (4):

$$OH + H^+ + e^- \rightarrow H_2O \quad (4)$$

For this reason, many works devoted to the treatment of different pollutants such as antineoplastic agents and cytostatics [34,35], antibiotics [36] or industrial wastewater [37,38] have chosen an acidic pH close to 3 as optimal conditions. Nonetheless, UV/Fe/H_2O_2 feasibility is severely limited by acid/base addition, which implies: (i) higher operational costs due to reagent's consumption, (ii) more complex operation due to the requirement of a neutralization step prior to discharge, and (iii) the increases in conductivity in the final effluent [39].

Among all the strategies for the intensification of the UV//Fe/H_2O_2 process, one of the most effective is the use of iron complexes to increase the phototonic efficiency and maintain iron in solution, even at circumneutral pH. In this regard, iron–organic complexes (Fe^{3+}-L) can maintain iron in solution at much higher concentrations at higher pH, and light can reduce Fe^{3+} to Fe^{2+} to form organic radicals (see Equation (5)), which can then participate in the formation of reactive radicals that favour pollutant degradation [40]:

$$Fe^{3+}\text{-L} + UV \rightarrow Fe^{2+} + L \quad (5)$$

Oxalic acid and citric are probably the most investigated iron ligands, as both present high quantum efficiencies and low toxicity [41]. However, these chelating agents leave mod-

erately acidic conditions in the effluent; thus, other alternatives such as ethylenediamine-N,N′-disuccinic acid (EDDS) have emerged as a promising alternative. In this regard, Silva et al. [42] assessed the performance of photo-Fenton at neutral pH in the presence of different organic iron complexes using hydrogen peroxide or persulfate as oxidants for naproxen degradation. As a main conclusion, the best results were observed in the presence of Fe/EDDS (1:1), although the Fe-citrate complex with H_2O_2 was the most cost-effective.

Heterogeneous photo-Fenton can also be considered as a solution to avoid acidic conditions, and in this regard, a wide range of materials including iron oxides, carbon, clays, and perovskites have been satisfactorily employed at neutral conditions. Examples include the treatment of tetracycline at pH_0 = 6 with $ZnFe_2O_4$ [43], the employment of Fe-g-C_3N_4/graphitized mesoporous carbon composite as an effective Fenton-like catalyst to treat Acid Red 73 in a wide pH range [44] or the employment of metallurgical slag as a Fenton-type photocatalyst for the degradation of diclofenac at pH 7 [45]. Obviously, working with heterogeneous systems is always a tricky situation, as several factors must be considered, i.e., mass transfer limitations, light penetration, catalyst stability, lower reaction rates, catalyst separation, etc.

Working at circumneutral pH can also be feasible using significantly low iron doses, even with natural iron present in wastewater, as the proposal of Buitrago et al. [46], who demonstrated that low amounts of iron, such as those typically found in natural surface or well water, are sufficient to remove amoxicillin operating the process at the initial pH ~ 7.0. Similarly, De la Cruz et al. [47], achieved removals of over 80% for 22 micropollutants in an effluent from a MWTP using Fe^{3+} concentration (1.6 mg·L^{-1}) working at natural pH (unmodified pH remained between 6–7).

Table 2. Intensification of UV-AOPs by pH optimisation.

Photocatalytical System	Target Pollutant	pH Conditions	Remarks	Experimental Remarks	Ref.
1% Mg-ZnO-Al_2O_3/UV-A/B	Caffeine	pH = 3.5, 4.5, 9.5	Photocatalytic activity was enhanced at pH of 9.5 and dramatically decreased at pH of 3.5 At pH > 8.41 (surface negatively charged), favours cationic adsorption	[Caffeine] = 20 mg/L. Cylindrical Pyrex immersion photoreactor (2 L). UV Hg lamp (400 W). T = 25 °C	[13]
Immobilized TiO_2/UVA	Nitrosamines in MWTP, river or eutrophic matrices	pH = 3.0, 5.5, 7.0, 9.5	Optimum pH highly dependent on the proportion and speciation of intermediates during oxidation of each nitrosamine	UVA photocatalytic reactor (Blacklight λ = 315–400 nm) = 0.67 mW/cm^2; T = 22 °C	[30]
TiO_2 NPs/UVA	Methylene blue	Synthesis pH = 1.6, 7.0 and 10	Synthesis pH determined pH_{PZC} photocatalyst Optimum degradation (97%, k = 0.018 min^{-1}) was achieved with TiO_2 NPs prepared at pH 10	1 L photoreactor with 6W Lamp (365 nm) The cell was filled with 0.6 L of 10 mg/L of MB and 100 mg/L of the photocatalyst; T = 25 °C	[31]
TiO_2/Solar	Phenol, dichloroacetic acid, pyrimethanil	Natural pH	At pH 2.7, titania (positively charged) and $CHCl_2COO^-$ (pKa = 1.26) interaction favoured direct DCA degradation. Conversely, indirect ·OH attack govern phenol removal (pKa = 9.9) at natural pH	CPC (Compound Parabolic Collectors) tubes (3.2 m^2 irradiated area) under turbulent flow conditions and solar light. V_T = 35 L	[32]

Table 2. *Cont.*

Photocatalytical System	Target Pollutant	pH Conditions	Remarks	Experimental Remarks	Ref.
H_2O_2/Fe^{2+}/UV	Antibiotics (amoxicillin, ampicillin and cloxacillin)	pH = 2.0, 2.5, 3.0, 3.5 and 4.	Maximum degradation was achieved at pH 3	600 mL Pyrex reactor equipped with a UV lamp (6 W) emitting at 365 nm. [AMX, AMP, CLX]$_0$ = ~100 mg/L, [COD] = 520 mg/L; [H_2O_2] = 16.25 mM	[36]
H_2O_2 or $S_2O_8^{2-}$/UV/Fe-complex (NTA, FeEDTA or FeCit, or FeOx)	Naproxen in a wastewater effluent collected in a MWWT	pH natural	Photo-Fenton at neutral pH was efficient for naproxen degradation in the presence of all iron complexes	Vis Xe high-intensity discharge lamp (X-HID) [NAP] = 1 µmol/L; [H_2O_2] = 16.3 mmol/L or [$S_2O_8^{2-}$] = 4.9 mmol;/Ligand [Fe^{3+}] = 21.4 µmol/L, pH = 7.5 (natural pH).	[42]
$ZnFe_2O_4$/UV/H_2O_2	Orange II	Initial at pH$_0$ = 3, 6, 7 and 9	Decolourization efficiency increased slightly with pH, optimum at pH = 6	Xe high intensity discharge lamp (X-HID) (454 nm and 150 W) 50 mL glass beaker [Orange II] = 100 mg/L, [H_2O_2] = 5 mM, [catalyst] = 0.5 g/L, T = 20 °C, pH$_0$ = 6)	[43]
Metallurgical slag as a Fenton-type photocatalyst	Diclofenac	Natural pH = 7	Complete depletion and a partial mineralization were achieved with the COB/H_2O_2/sunlight system at pH 7	[Diclofenac] = 500 mg/L, Sunlight simulator with Xe arc lamp (500 W/m^2) pH = 7, [H_2O_2]$_0$ = 180 mg/L, 1:18 mass ratio of Fe/H_2O_2.	[45]
Fe^{3+}/H_2O_2/UV	Diuron and amoxicillin	Pollutants exhibited a strong degradation keeping the circumneutral pH	Presence of anions (HCO_3^{2-}, HCO_3-, humic acids . . .) leads to photo-chemical reactions (dissolved ferric–humic acid complexes, colloidal iron . . .) at circumneutral pH	Solar simulator (300 W/m^2) [amoxicillin] = 10 mg/L humic acids (HA) = 2.0 mg/L; [carbonates] = 100 mg/L; [Fe^{3+}] = 0.3 mg/L, [H_2O_2] = 15.2 mg/L, pH$_0$ = 7.0	[46]
UV/H_2O_2 and neutral photo-Fenton	22 micropollutants (including 15 pharmaceuticals) in MWTP	Natural pH	Fe addition to the reactor did not improve the process; degradation was higher using uniquely the Fe present in water (1.6 mg/L)	Continuous operation Reactor 5 LP Hg lamps (254 nm, 150 W each); V = 37 L	[47]

2.3. Temperature

In general terms, because of the relatively low activation energy of photocatalytic reactions in contrast to other conventional reactions, the effect of temperature on reaction rate is not so significant. However, certain aspects must be considered, and many studies have analysed the effect of temperature for the optimisation of operating conditions in UV-AOPs (see Table 3). When temperatures are too high (above 80 °C), the adsorption capacity of the solid is reduced and the oxygen solubility in the solution decreases, while electron–hole recombination is preferred [10]. On the contrary, at low temperatures, desorption becomes the limiting step.

In any case, the temperature will increase the photodegradation within a certain range; thus, there is a certain margin for the boosting of heterogeneous photocatalytic processes by temperature. In this regard, Tambat and co-workers [48] studied Milling yellow photocatalytic degradation with a CeO_2 catalyst; they observed that complete degradation was possible by increasing the temperature from 20 to 35 °C, while an only slightly increased degradation rate was observed heating up to 60 °C. Lin and co-workers [49] found similar behaviour in the decolourization efficiency of Red MX-5B dye by UV-A with a TiO_2/Ag catalyst, where higher reaction rates were achieved, increasing the operating temperature to 40 °C, although at 50 °C, the process efficiency decreased slightly due to the

acceleration of electron–hole recombination. Chen and Hsu [50] investigated the effects of reaction temperature on the photocatalytic activity of TiO_2 with cocatalysts of Pd and Cu, concluding that when the reaction temperature is higher than 70 °C, the recombination of charge carriers will increase. For its part, the temperature on nitrate photoreduction with ilmenite was studied in the range of 20–80 °C by Silveira and co-workers [51]; in this case, the authors observed increases in reaction kinetics throughout the temperature range. Increasing temperature diminishes oxygen solubility, which could make photoreduction more feasible, avoiding the need to use inert gas flow to remove O_2 in solution.

Jonathan Z. Bloh [52] argues that in UV/TiO_2 systems, the temperature dependence becomes apparent only at high light irradiation intensities, but that under these conditions, the kinetic bottleneck at the particle occurs due to mass transfer and catalysis surface/or limitations. Thus, effective intensification towards the industrial implementation of UV/TiO_2 at significantly high temperature could only take place by optimization of the photophysical properties of photo-absorber materials (i.e., avoid mass transfer limitations and optimizing substrate surface). However, to this day, in heterogeneous photocatalysis, temperatures of up to 50–80 °C can be considered the ideal temperature for photocatalytic optimisation [10,50].

For its part, in photo-Fenton and UV-Fenton-like processes, temperature plays an important role on reaction rate (see Table 3); thus, appropriate temperature selection may be used for intensification purposes [53]. Many works have reported the increase in reaction rate by temperature, including several applications such as industrial textile wastewater treatment [54,55], nitrophenol removal [56], alachlor degradation [57] or phenolic effluent treatment by heterogeneous photo-Fenton with a Fe_2O_3/Al_2O_3 catalyst [58]. Additionally, moderately high temperatures (up 65 °C) may contribute to synergistic treatment of industrial beverage effluent by the photo-Fenton process intensified by activation of persulfate [59].

Few authors have also observed adverse effects when the temperature increases above a certain value. In this regard, Zapata and co-workers [60] assessed the influence of temperature on photo-Fenton degradation to treat commercial pesticides, while increasing the temperature from 25 to 42 °C required a substantial extension of mineralisation (up to 70%) at shorter irradiation times with more efficient use of hydrogen peroxide, a dramatic decline in mineralisation of DOC was observed at 50 °C. The authors attributed this behaviour to a significant loss of iron by precipitation in the studied conditions.

In any case, a relatively limited number of papers have explored the effect of temperature beyond 50 °C, and it seems that further exploration of the intensification by temperature in photo-Fenton processes could be worthwhile. Thus, Carbajo and colleagues [61] studied the possibility of intensifying homogeneous photo-Fenton by increasing the temperature (up to 90 °C) to treat a real leachate effluent of landfill using the stoichiometric amount of H_2O_2 (2.12 g/g COD) and 10 mg·L^{-1} of Fe^{2+}. The required irradiation time to achieve maximum TOC and COD removals (around 80%) was reduced from 180 to 45 min by increasing the temperature from 50 to 90 °C, and the irradiation efficiency increased four-fold within this temperature range. Furthermore, according to the authors, operating costs at high temperatures more than offset the costs due to wastewater heating; thus, working at 90 °C results in a three-fold reduction of the costs observed at 50 °C.

2.4. Oxidants

In UV/Fe/H_2O_2 processes, increasing the concentration of H_2O_2 concentration usually led to an increase in reaction rate. Although excess H_2O_2 may marginally increase the reaction rate and worsen the efficiency of H_2O_2 consumption, the last can be attributed to scavenging reactions where H_2O_2 competes for hydroxyl radicals, with organic matter producing less powerful radicals (see Equation (6)):

$$H_2O_2 + HO^{\bullet} \rightarrow HO_2^{-} + Fe^{3+} \quad (6)$$

Working with poor hydrogen peroxide conditions may also be inappropriate, as it limits the degree of mineralisation and slows down the reaction rate. Therefore, as can be seen in Table 4, many authors have tried to optimise the use of the amount of oxidant to intensify the UV-AOPs processes.

Usually, the first approach to increase the efficiency of a particular process consists of testing the theoretical stoichiometric amount of H_2O_2 required to completely remove COD or TOC, which are found to be appropriate conditions in some cases [62], although many authors have found optimal conditions working below the stoichiometric conditions to minimise H_2O_2 consumption. For example, in complete degradation of persistent antidepressant sertraline in aqueous solution by solar photo-Fenton, TOC removal was achieved up to 90% with 40% of the stoichiometric amount of H_2O_2 [63]. In addition, substoichiometric amounts of H_2O_2 can be enough to increase the biodegradability of wastewater containing recalcitrant or inhibitory pollutants when photo-Fenton is used as a pretreatment before a biological process.

More typically, an over-stochiometric H_2O_2 dosage is expected when the characteristics of the wastewaters are required, for example, when parallel reactions and inefficiencies occur in the process due to typical ions present in real wastewaters such as Cl^- or $CO_3{}^{2-}$ which react with OH radicals to give less powerful radicals (Cl, $CO_3{}^-$, . . .) [64–66]. Some examples are found in optimisation of the treatment of landfill leachate by photo-Fenton [67], where the use of stoichiometric excess H_2O_2 (up to 4, 5 times) was required to achieve a higher degree of mineralisation of acetylsalicylic acid, decreasing energy-related costs [68]. Similar assumptions have been reported for sulfonamide antibiotics derived from sulfanilamide [69], the degradation of antibiotic mixtures (amoxicillin, ampicillin, and cloxacillin) in aqueous solution, and the treatment of reverse osmosis retentate from a paper mill [64].

Optimization of UV/Fe/H_2O_2 can also be carried out by H_2O_2 dosing. In this regard, the sequential addition avoids high instantaneous concentrations of H_2O_2, minimising unproductive reactions (see Equation (5)) and increasing its consumption efficiency. In this context, the sequential addition of H_2O_2 along the reaction has been reported to improve mineralisation in several works [70–72]. Furthermore, continuous automatic dosage has also been studied with positive results [17], and recent work focusses on finding dosage models and methodologies to optimise hydrogen use [73] or employing (Yu et al., 2020) [68] indirect measurement of H_2O_2, such as evolution of O_2 concentration, for continuous oxidant monitoring dosage [74]. In conclusion, the dose of H_2O_2 must be carefully balanced for each type of wastewater, the dose of iron, and the goal of decontamination in order to intensify the process, i.e., improve kinetics and maintain the best possible efficient oxidant consumption, which is by far the largest operational cost in solar photo-Fenton [75].

UV/Fe processes may also be intensified by the combination of or the use of alternate oxidants. A good example of this is the work of Devi et al. [76], where zero-valent metallic iron (Fe^0) was employed in photo-Fenton methyl violet degradation comparing ozone, peroxymonosulfate (PMS) and peroxydisulfate (PDS) with classical hydrogen peroxide (HP). PMS was found to be a better oxidant compared to H_2O_2 and PDS under higher pH conditions. For its part, Silva et al. [42] concluded that naproxen removal in distilled water was faster in the presence of H_2O_2 compared to $S_2O_8{}^{2-}$; they believed that better performance of $S_2O_8{}^{2-}$ was observed in sewage treatment plant effluent.

O_2 acts as a low-cost acceptor for conduction band photogenerated e and is the most common oxidant in UV/TiO_2 systems, as it can be adsorbed on titania from the liquid where it is dissolved following Henry's law by simple aeration systems. However, the process of optimization of UV/TiO_2 may include the use of alternative electron acceptors in the reaction to increase the number of trapped e^- inhibiting recombinations that form more powerful radicals [77]. For example, the introduction of persulfate into the TiO_2 photocatalytic system can increase the separation of electron–hole pairs simultaneously generating sulfate radicals ($SO_4{}^{\bullet-}$), characterised by high redox potential and longer half-life times [78]. Many works have explored this strategy, including elimination of

sulfaclozine from water with $SO_4^{\bullet-}$ radicals [79], the degradation of ibuprofen by UVA-LED/TiO_2/persulfate processes [80] or the visible-light activation of persulfate by TiO_2/g-C_3N_4 photocatalyst in the degradation of micropollutants [81]. H_2O_2 has also been used satisfactorily as a powerful oxidising agent to inhibit e^-/h^+ recombination. Good examples of this strategy are the dosage of H_2O_2 during the photocatalytic degradation of ethidium bromide with iron-doped TiO_2 catalysts, where the authors observed a significant increase in the mineralisation of ethidium bromide due to the minimisation of self-scavenging reactions [82], or the heterogeneous photocatalytic degradation of pharmaceuticals in synthetic and real matrices using a tube-in-tube membrane reactor with radial addition of H_2O_2 [83].

Table 3. Intensification of UV-AOPs by temperature optimisation.

Photocatalytical System	Target Pollutant	Temperature Conditions	Remarks	Experimental Remarks	Ref.
TiO_2/Ag	Procion red MX-5B	R.T. to 50 °C	Operating temperature increased decolourization efficiency from R.T. to 40 °C but decreased at 50 °C as e^-/h^+ recombination accelerates	Photoreactor V_T = 0.5 L; Lamp: 10-W UVA (0.7 μW/cm^2); [MX-5B] = 30 ppm	[49]
TiO_2, Pd/TiO_2 or Cu/TiO_2	Methylene blue	0 to 70 °C	At 0–50 °C, TiO_2 and Pd/TiO_2 activity increased with temperature; at 70 °C, rate dropped slightly or became less effective due to recombination rate increase	UVC lamps (λ = 254 nm), TUV PL-L 18 W. V_T = 20 mL; [MB] = 10 mg/L	[50]
$FeTiO_3$	NO_3^- in saline water	range of 20–80 °C	73% total nitrogen reduction was reached at 420′ An increase in the temperature enhanced reaction kinetics. At high T, N_2 bubbling to maintain inert conditions is avoided (lowering O_2 solubility)	Set-up: Magnetically stirred glass jacketed batch reactor (V_T = 700 mL). Lamp: 150 W M.P. Hg lamp (30 W/cm^2) Working at [$C_2O_4^{2-}$] = 180 mg/L, [$FeTiO_3$] = 450 mg/L; [HCl] = 13 mM,)	[51]
UV–Vis/H_2O_2/Fe(II)	Textile effluents	25 to 70 °C	Temperatures above 25 °C and up to 70 °C show a beneficial effect on organic load reduction	Lamps: 6 W Black-light and 250 W Xe and Solar light.	[55]
Solar/H_2O_2/Fe(II)	Alachlor	20 to 50 °C	At best operating conditions (maximal iron concentration 2.6 mM, maximal temperature 70 °C) an increase reaction rate 5-fold by raising temperature from 20 to 50 °C	Pilot-plant CPC sunlight operated in batch mode. Collector (CF = 1): 20 Pyrex tubes (Øin = 46.4 mm). $A_{collector}$ = 4.16 m^2, Vi = 44.6 L	[58]
Solar/H_2O_2/Fe(II)	commercial pesticide mixture	25 to 50 °C	Photo-Fenton efficiency gradually rose with temperature; nevertheless, at 50 °C, efficiency decreases	Pilot-plant CPC with sunlight operated in batch mode. Collector (CF = 1): (Øin = 50.0 mm). $A_{collector}$ = 1.04 m^2 20 Pyrex tubes; Vi = 44.6 L [DOC] = 200 mg/L (40 mg/L of each commercial pesticide); pH = 2.7–2.9; [H_2O_2] = 100 to 300 mg/L	[61]
UV/H_2O_2/Fe(II)	Phenolic and landfill leachate wastewater	25 to 90 °C	Time to achieve maximum TOC and COD removals (80%) was reduced from 180 to 45 min from 50 to 90 °C. Irradiation efficiency increased 4-fold within this range	immersion-wall batch jacketed 1 L photoreactor; Lamp: 150 W MP Hg. pH = 2.7–2.9; [H_2O_2] = 100 to 300 mg/L; Fe^{2+} = 10 ppm	[62]

Table 4. UV-AOPs intensification by oxidant usage optimization.

Photocatalytical System	Target Pollutant	Oxidant Type and Conditions	Remarks	Experimental Remarks	Ref.
UV–Vis/H_2O_2/Fe(II)	mixture of 6 emerging pollutants	Stoichiometric H_2O_2 to mineralize mixture (146 mg/L)	Data show that photo-Fenton in high-salinity wastewater at pH = 2.8 and pH = 5.0 was capable to remove all pollutants in 1 h	50 W xenon lamp on open glass reactor; borosilicate glass [Emerging pollutants] = 5 mg·L^{-1} each; [Fe] = 5 mg·L^{-1}	[63]
UV–Vis/H_2O_2/Fe(II)	sertraline	[H_2O_2] = 10–100% Sub-stoichiometric amount	TOC removal up to 90% was achieved at a hydrogen peroxide dose as low as 40% of the stoichiometric amount for mineralization	Lamp: Xenon 550 W m^{-2} (300 to 800 nm). Vr = 500 mL; [Sertraline] = 50 mgL^{-1}. The [Fe^{2+}] = 1–10 mgL^{-1}; [H_2O_2] = 10–100% stoich amount	[66]
UV–Vis/H_2O_2/Fe(II)	Acetylsalicylic acid	[H_2O_2] = Up to 9-fold the stoichiometric Amount	Mineralization around 90% is reached at 10 min with 4.5-fold excess of H_2O_2	2 Parabolic tubular modules in series, Lamp: Black-light UVA (40 W) [Fe^{2+}] = 1.5 mM; [H_2O_2] = 45 Mm [Acetylsalicylic acid]$_0$ = 100 ppm	[69]
UV–Vis/H_2O_2/Fe(II)	Orange II (OII)	Continuous addition of H_2O_2	H_2O_2 continuous dosage optimize photocatalytic efficiency (scavenger effect is minimized); 100% decolouration (95% TOC removal) with continuous addition of peroxide	Solar reactor (50 L); Ai = 2 m^2 (CF = 1); 16 borosilicate-glass tubes (OD = 32 mm) Fe(II) = 2 ppm; Orange II = 20 ppm,	[72]
H_2O_2 or $S_2O_8^{2-}$/UV/Fe-complex (NTA, FeEDTA or FeCit, or FeOx)	Naproxen in a sewage effluent collected at a MWWT	H_2O_2 compared to $S_2O_8^{2-}$	H_2O_2 best performed in ultrapure water, while $S_2O_8^{2-}$ best performed with real WW	Lamp: Xe high int. discharge [NAP] = 1 μmol/L; [H_2O_2] = 16.3 mmol/L or [$S_2O_8^{2-}$] = 4.9 mmol; Ligand [Fe^{3+}] = 21.4 μmol/L, pH = 7.5 (natural pH).	[42]
TiO_2/g-C_3N_4	Acetaminophen	PS dosage increases from 0.5 mM to 2 mM	The addition of PS greatly improved the degradation efficiency (5 mg/L AAP almost degraded; at 30 min; k = 0.061 min^{-1}, X_{TOC} = 82.5%)	Lamp: Xe (300 W, 400 nm cutoff filter) [TiO_2/g-C_3N_4] = 500 mg/L, [AAP] = 5 mg/L [PS] = up to 2 mM	[82]
TiO_2/Fe-TiO_2	Ethidium bromide	[H_2O_2] = 80–160 mg/L, 1–2-fold stoichiom, and continuous dosification was evaluated	196 mg/L H_2O_2 addition was optimized throughout; several dosages maintaining H_2O_2/TOC ratio; performance was maximized, raising 84% of TOC conversion	Pyrex photoreactor with a Hg MP lamp (500 W); Vr = 1 L, [EtBr] = 20 mg/L, [Fe-TiO_2] = 500 mg/L, pHo = 3, [H_2O_2] Total = 196 mg/L	[83]

3. Catalysts Engineering

As part of photo-assisted process intensification, a solid/heterogeneous photocatalyst is commonly required to perform the oxidative treatment of polluted water matrices.

In an archetypical photocatalytic process, the semiconductor par excellence is the titania (TiO_2) due to its properties (good stability and relevant optical and electronic properties). However, its employment has been reduced due to the necessity of UV light for excitation.

In this sense, in this part of the review, the catalysts devoted to act with a double role, thus named bifunctional catalysts, will be considered.

In recent years, many efforts have been made for the development of photocatalytic materials, a key piece for intensifying the entire process. Overall, optimisation has been carried out in two preferred directions, one mainly affecting the physical limitations of the reaction and the other affecting the overall yield of the treatment, also related to the chemical limitations. Until now, the main approaches performed for the intensification of the photocatalysts are globally divided into two elements (Figure 3):

(a) Photocatalyst design is orientated to reduce the limitations in mass and photon transfer. This strategy can be achieved via three steps as follows:
   - Improving photocatalyst activation and preventing deactivation. This fact is related to the shift of the absorption edge from the ultraviolet to the visible range. This item has been extensively studied; thus, it will not be developed as a separate alternative in this review unless combined with other sorts of intensifications.
   - Promotion of the adsorption of reagent onto the catalyst surface: the initial step of a Langmuir–Hinshelwood model.
   - Promotion of the desorption of reactions products from the catalyst: The last step of a Langmuir–Hinshelwood model.

(b) Design of bifunctional catalysts favouring the increase in oxidant species generation yield (mainly $HO_x\cdot$). In the same way, two steps have been performed for this purpose:
   - The combination of several single processes without oxidant addition.
   - The extra-addition of oxidant agent.

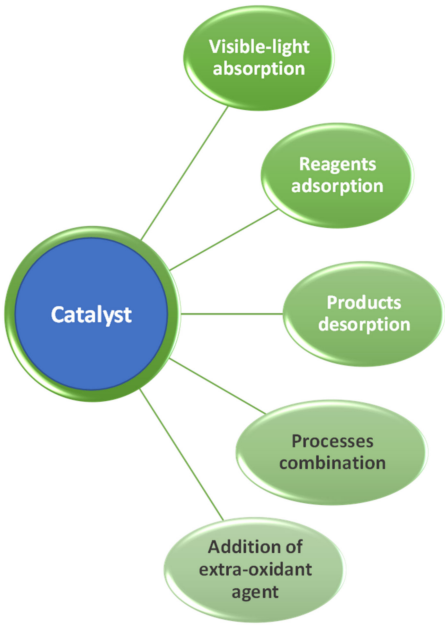

Figure 3. Main strategies developed for process intensification via photocatalyst.

Those strategies are further detailed including the main approaches found in the bibliography for each one of them.

3.1. Design Oriented to Reduce the Physical Limitations

In this part, the mass and photon transfer limitations are meant to be overcome. As mentioned above, the photon absorption strategy will not be developed here due to the large number of works dealing with the visible-assisted photocatalysts existing in the literature. In terms of mass transfer, the issue proceeds with the obtention of photocatalysts characterised by a higher adsorption capacity. This combination favours the initial pre-stage of a Langmuir–Hinshelwood model, typically established in photo-assisted processes. Among the strategies chosen to increase the initial adsorption of the pollutants, the development of mesoporous materials has been elected as the preferred one, not only

due to the diffusion of pollutants within the pores in some cases, but also associated with the anchorage of the active phase in the pores of a support, which leads to an inhibition of pollutant diffusion in some cases and therefore to improved photoactivity [84–89]. In addition, we can find works dealing with a direct increase in the surface of the support or works in which the surface has been chemically modified to promote this initial stage [90]. Some work has been reported following these approaches in which a true synergistic effect was demonstrated (Table 5).

Finally, the last and less used strategy consists of chemical modification of the material based on the Bronsted and Lewis acid sites to promote the catalyst–substrate interaction, as was obtained with the $SO_4^{2-}/Fe_{2-x}Zr_xO_3$ catalyst for the photo-Fenton process. The conditions and processes involved are given in detail in Figure 4.

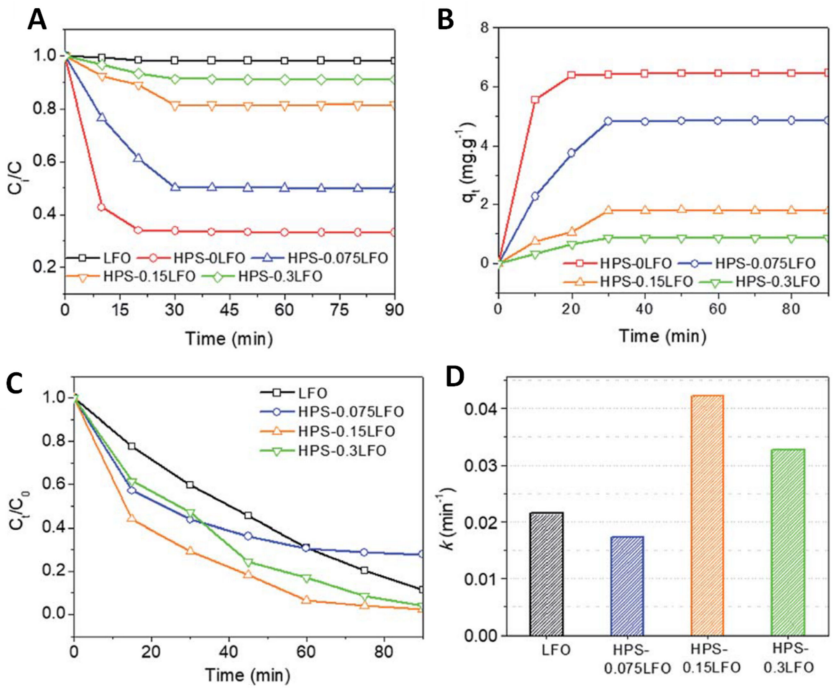

Figure 4. (**A**) Removal of RhB via adsorption by using LFO or HPS_xLFO. (**B**) The corresponding RhB adsorption capacity. (**C**) Removal of RhB in the photo-Fenton reaction using LFO or HPS-xLFO (x = 0.075, 0.15, and 0.3) and (**D**) corresponding degradation rate constants. Operating conditions: T = 25 °C, initial dye concentration = 10 mg/L, catalyst dosage = 1 g/L, initial H_2O_2 concentration = 10 mM and pH_0 = 6). Reproduced with permission from Ref. [87]. Copyright of Royal Society of Chemistry.

In one case, the active phases of the catalysts were immobilised onto surfaces established by a certain porosity. The authors achieved catalytic activities towards pollutant depletion that were higher than those in reactions in which the catalyst was nonsupported. The improvement was basically attributed to two effects: (i) an increase in the amount of adsorption itself and (ii) an enhancement in the transfer of photocharges. Several works have used $LaFeO_3$ as active phase and zeolite [88], silica [87] and resin [91] materials as supported materials (Table 5). In the second case, the mesoporosity was created inside the photocatalyst itself, leading to the configuration of binary materials, e.g., heterojunction. In these cases, in addition to a favoured adsorptive attraction, a substantial increase in oxidation rates was observed. The development of the B/Bi_2WO_6, Au/TiO_2, Fe_2O_3/TiO_2 and Ga_2O_3/TiO_2 mesopores follows with the improvement in charge transfer and the change of the absorption edge towards visible and infrared regions (Figure 3).

In terms of optimisation via the promotion of the product desorption from catalysts, there is evidence that the joint employment of AOP-ultrasound can benefit this step of the process, letting the active phase again be available to the new reactants. However, this

combination has not been developed specifically to overcome this limitation. For that, the use of ultrasound will be explained in the following sections of this review.

Table 5. Catalyst used for combining adsorption and photo-assisted processes.

Catalyst	Processes Involved	Light Spectra	Pollutant	Conversions	Advantages	Disadvantages	Ref.
B/Bi_2WO_6	Adsorption/ photocatalysis	Solar	Rhodamine B	B/Bi_2WO_6 = 8.8 k Bi_2WO_6 X_{RhB} = 100% (180 min)	Mesoporous favours adsorption. B presence creates higher pore volume related to mesopores B acts also as electron trap	No TOC	[84]
$LaFeO_3$/Zeolite	Adsorption/ photo-Fenton	Visible	Rhodamine B		Higher adsorption and active sites	No evaluation of TOC parameter	[88]
$LaFeO_3$/Silica	Adsorption/ photo-Fenton		Rhodamine B				[87]
Mesoporous Au/TiO_2	Adsorption/ photocatalysis	Visible	AO7 (dye)				[89]
SO_4^{2-}/ $Fe_{2-x}Zr_xO_3$	Adsorption/ photo-Fenton	Visible					[90]
$LaFeO_3$/Resin	Adsorption/ photo-Fenton/ photocatalysis	Solar	Caffeine (CECs)	80% removal caff in 3 h 60% TOC	Reusability until 6th cycle	Not a complete mineralization	[91]
Mesoporous Fe_2O_3-TiO_2	Adsorption/ photo-Fenton/ photocatalysis	Visible	Norfloxacin antibiotic	100% removal and 97% mineralization in 120 min	Good reusability. New reactor designed with LED light	Low iron leached.	[85]
Mesoporous Ga_2O_3-TiO_2	Adsorption/ photocatalysis	UV	Imazapyr pesticide	98%removal in 180 min	10 and 3 times more activity than Ga_2O_3 and UV100	Loss of activity in 5 cycles	[86]

3.2. Design of (Bifunctional) Catalysts Favouring the Increase in Oxidant Species Generation Yield (Mainly HO_x)

This approach mainly focusses on the development of photoactive materials capable of demonstrating activity, leading to an increase in the generation of oxidising species and thus provoking higher reaction yields in terms of pollutant removal. In the literature, there exists numerous ways of classifying this part; nevertheless, all of them converge in the concept that the synergy is formed by a main process and another contribution that can be either a well-established process or the addition of an extra external oxidising agent.

The increase in the number of reactions devoted to the production of radicals and capable of depollating is the basis of this approach. There are diverse and varied combinations of techniques to promote radical generation: photocatalysis/photo-Fenton, photocatalysis/persulfate activation, photocatalysis/ozonation, or photocatalysis/ultrasound, etc. Among them, this review will focus on those processes in which the catalyst constitutes a key piece for the combination: microwave/photocatalysis, photo-Fenton/photocatalysis, and persulfate addition to photocatalysis.

3.3. Wave-Assisted Photocatalysis

Another approach for intensifying the role of a catalyst is using different kinds of waves. There have been two wave-types mainly reported that are characterised by a different nature and by a varied energetic level of them, and these are ultrasound and microwaves. In the case of ultrasound, the mechanical wave employed has an energy

higher than 20 KHz, and in the case of microwaves, the electromagnetic waves are inside the range of 300 MHz to 300 GHz. Despite this important difference, the treatments are generally mentioned as a wave-irradiated process.

One of the first studies reporting the use of a heterogeneous photocatalyst, TiO_2, for this dual process was carried out by the Gogate group [92]. The general basis consists of the creation of localised higher energy and uniform heating that leads to a reduction of the activation energy and bond cleavage of organic molecules. They studied the combination of several AOPs in addition to microwave implementation. The most active synergy resulted from the simultaneous application of microwave, photocatalysis, and H_2O_2 addition. Since microwave irradiation and photocatalysis act via a similar mechanism, their combination suggests a better performance in terms of efficiency. In this work, for the concrete case of microwave and photocatalysis, the reaction rate for the removal of pollutants increased from 6.2×10^{-3} to 3.88×10^{-3} min^{-1}, meaning an improvement of 1.6 in terms of reactivity and passing from 15% to 67% of the oxidation percentage. In another work, a simple modification of a raw titania photocatalyst was developed by N doping to shift absorption spectra into the visible range [93]. Furthermore, titania was coupled to activated carbon and used for the removal of tetracycline antibiotics by a hybrid process [94]. A total synergetic effect was demonstrated with a pollutant removal of 93% and half the mineralisation of the effluent in 180 min of sonophotocatalytic reaction.

As an example of a ternary photocatalyst, CuO-TiO_2/rGO in ultrasonic photocatalysis can be considered [95]. The gain in this case was 3.7 times. The catalyst was used for the removal of methyl orange dye under UV light with a 99% depletion of methyl orange in 90 min, but no TOC evaluation was performed. The last example of this combination deals with the use of a quaternary catalyst, Fe_3O_4/TiO_2–N-GO for ultrasonic photocatalysis. The combination reports several advantages related to different effects. First, ultrasounds favour the catalyst dispersion and thus improve the mass transfer inside the reaction media. Second, ultrasound can generate extra $HO^{\bullet}$ due to a cavitation effect. Bubbles collapse, leading to high pressure and temperature conditions, provoking the breakdown of H_2O or O_2 molecules on oxidising radicals. These radicals can recombine and produce H_2O_2, which can be taken for a heterogeneous Fenton process. Thus, the Fe_3O_4/TiO_2–N-GO catalyst allows one to take advantage of all the reasons mentioned above with efficiencies higher than 26% compared to the pure photocatalytic system [96]. Recently, another quaternary photocatalyst, N-Cu co-doped TiO_2@CNTs, was developed and employed for the treatment of antibiotic-containing real pharmaceutical wastewater and under UV–visible light. In this case, total depletion of the pollutant was reached with great yields: 93% COD and 89% TOC [97]. The catalyst showed certain stability with a lifetime of more than five cycles of reaction. A full list of works can be found in Table 6.

3.4. Synergistic Effect: Photocatalysis/Photo-Fenton

Photocatalysis/photo-Fenton represents one of the first and most widely used combinations in AOP treatments. The reasons are that the combination provides the advantages of one process with respect to the drawbacks of the other. While photocatalysis allows for total mineralisation of the effluent as a final achievement, the Fenton process provides the drive-in reaction rate to be competitive with other nonadvanced processes. Furthermore, the combination provides a greater number of redox reactions that deal with the increase in the overall yield, not only due to the generation of a radical, but also associated with the capture of the photogenerated charges by H_2O_2 that leads to the inhibition of recombination of the charges, a highly requested issue for the enhancement of the photocatalyst activity.

Table 6. Catalysts devoted to the combination of radiation and photocatalysis.

Catalyst	Processes	Conditions	Pollutant	Yield	Advantages	Disadvantages	Ref.
CuO-TiO_2/rGO	Ultrasound/ photocatalysis	UV light	Methyl orange	99% oxidation in 90 min	Synergy of 3.7 times	No TOC evaluated. Reduction of activity with the reuse	[95]
Fe_3O_4/TiO_2–N-GO	Ultrasound/ photocatalysis	Visible light	Humic acids	93% removal	Surface cleaning, improved mass transfer. 26% higher removal compared to single photocatalysis		[96]
N-Cu co-doped TiO_2@CNTs	Ultrasound/ photocatalysis	Xenon lamp	Sulfamethoxazole in real pharma-ceutical wastewater	100% antibiotic 93% COD 89% TOC	Real pharmaceutical water	Reuse until 6th cycle	[97]
TiO_2 decorated on magnetic activated carbon	Ultrasound/ photocatalysis	UV light	tetracycline	93% removal 50% TOC in 180 min		Fe leached measured	[94]
N-doped titania	Ultrasound/ photocatalysis/ filtration	Visible light	Dye	Synergetic effect higher than 20%	Ultrasonic cleans the membrane		[93]
TiO_2	Microwave/ photocatalysis	UV	4-chloro-2-aminophenol	Improvement in removal of more than 50%	Reaction rates of more than one order of magnitude	High energy consumption	[92]

A huge amount of new catalytic materials that increase the movement of charges have been developed in recent years, such as binary, doped, heterojunctions, or recently, network-substituted materials. The most representative photocatalysts and their reaction yields are shown in Table 7. As can be observed, by using this combination, higher depollution grades are obtained compared to the yields achieved by other hybrid processes. In all cases, removal percentages over 90% are reached for the main pollutant. In Table 5 are indicated the main catalysts that have been reported by their employment in the photocatalysis/photo-Fenton process. All of them are characterised by the presence of iron as the main active phase associated with the Fenton part of the process and by its implication as a visible light absorber for the photocatalysis part.

The preferred types of catalyst are heterojunction materials, probably because of the improved charge separation that enables higher reactivity. In this case, several binary and ternary junctions have been reported: $FeVO_4$@BiOCl [98], $LaFeO_3$/BiOBr [99], FeOOH/Bi_2MoO_6 [100], CQDs/FeOOH [101], TiO_2/Graphene oxide/Fe_3O_4 [102] and Fe-Cu oxide/diamond [103]. Ilmenite is formed by two phases: $FeTiO_3$ and rutile provoking a natural heterojunction ready to be used in this hybrid treatment [104]. As a second approach, the doped catalysts exist where graphene oxide remains as the main photocatalyst, and Fe_2O_3 and Fe_3O_4 are inserted into its network to activate H_2O_2 [105,106]. Recently, the last option used for the photocatalytic/Photo-Fenton process is the substitution of the network in the crystal structure, as in $La_{1-x}Ti_xFeO_3$ [107,108] (Figure 5) and $Zn_{1-1.5x}Fe_xS$/g-C_3N_4 [109]. The complexity of the synthesis to control the percentage substitutions is the reason for the low number of works inside this approach.

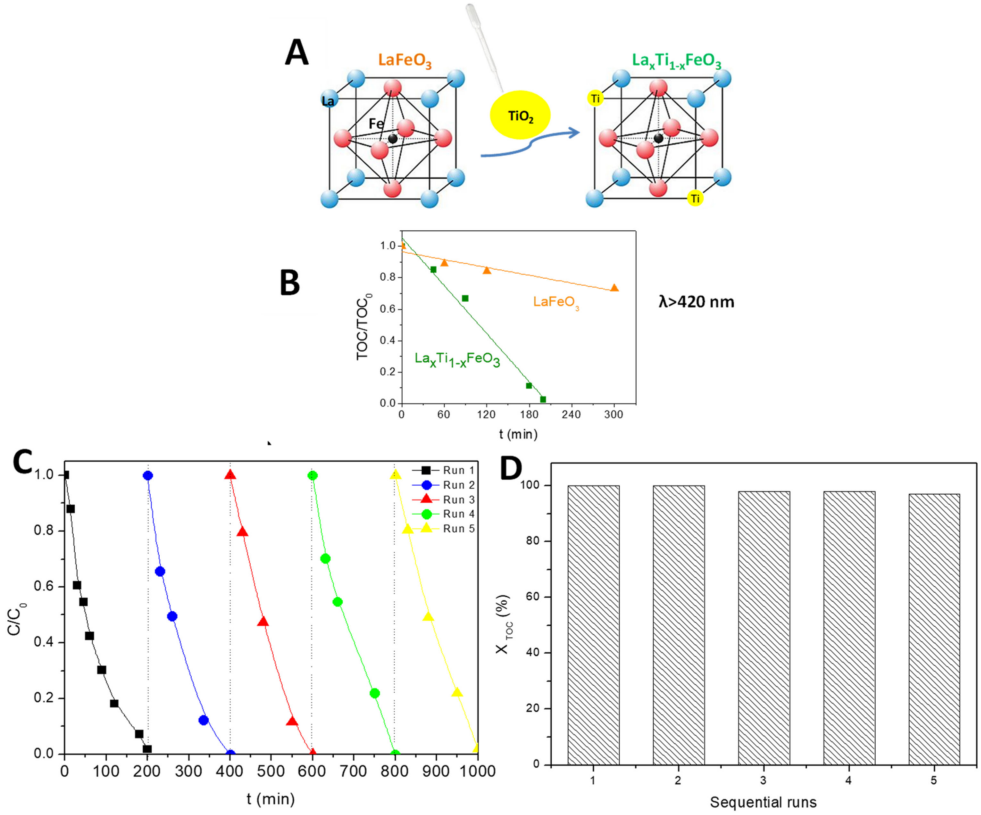

Figure 5. (**A**) Partial substitution of TI by La $LaFeO_3$ crystal structure and (**B**) the resulting TOC removal rate improvement under pure visible light (λ > 420 nm). Reproduced with permission from Ref. [108]. Copyright Elsevier. Reusability tests performed on the $La_{1-X}Ti_XFeO_3$ dual catalyst in the system H_2O_2/visible light: (**C**) Evolution of the relative 4-Chlorophenol concentration and (**D**) TOC mineralization degree obtained after 210 min of test. Operating conditions: $[4\text{-Cl-Phenol}]_0$ = 25 mg/L; $[H_2O_2]_0$ = 125 mg/L; T = 25 °C; [cat] = 0.5 g/L; (λ > 420 nm). Reproduced with permission from Ref. [108]. Copyright Elsevier.

3.5. Persulfate Addition to the Photo-Assisted Process

For the photo-assisted persulfate activation, single, binary, and ternary catalysts have been employed. Despite the substantial increase in mineralisation yield coming from the decomposition of persulfate into a hydroxyl radical and a sulfate anion, the strategy associated with the catalyst design also plays a key role in terms of process efficiency. In Table 8, the most relevant results taking place via catalyst are depicted [110].

For single-phase catalysts, two works have demonstrated an enhancement upon the activity. Zinc oxide and ilmenite ($FeTiO_3$) mineral were used for the activation of the light of persulfate. In the first work, 92% TOC removal was achieved in 1000 min of irradiation under sunlight, while in the second, 96% in 180 min by using ultraviolet light. The main advantages were the improvement in the reaction rates and the final mineralisation degree, while the drawbacks were concerned with all persulfate-treated water and the presence of higher residual sulphate in the solution. In the case of Ilmenite $FeTiO_3$, no leached iron was detected during the reaction time. When binary catalysts are used, the synergy is greatly increased in comparison to single materials. For example, TiO_2/g-C_3N_4 achieved 13 times greater activity than in the absence of persulfate and Co-$Bi_2Fe_4O_9$ more than 3 times compared to the doped catalyst. The last work involving a ternary material, Ag/AgBr/$ZnFe_2O_4$, obtained double reactivity towards the pollutant depletion with a value of 53% under visible light.

Table 7. Catalysts devoted to the combined photocatalytic-photo-Fenton processes.

Catalyst	Processes	Conditions	Pollutant	Yield	Advantages	Disadvantages	Ref.
Fe_2O_3 doped-C_3N_4	Photocatalysis-photo-Fenton	Visible light	Dicamba pesticide		LEDs light	No TOC measured	[106]
$FeVO_4$@BiOCl	Photocatalysis-photo-Fenton-sonophotocatalysis	UV light	p-nitrophenol	89% mineralization in 40 min	Additional OH· by the V^{5+}/V^{4+} cycle	Stability decreased from the 6th cycle	[98]
$LaFeO_3$/BiOBr	Photocatalysis-photo-Fenton	Sunlight	Rhodamine B	99.6% removal RhB in 30 min	Kinetic constant rate is 21 times higher than LFO	Stable just until 4th cycle	[99]
FeOOH/ Bi_2MoO_6	Photocatalysis-photo-Fenton	Visible light	Phenol	100% removal phenol (3 h)	Synergy: removal 1.54 higher than photocatalysis 1.33 higher than Fenton O vacancies improved photocatalysis	After 5th cycle a step decrease in activity Iron leached detected. 48% TOC removal	[100]
Carbon quantum dots/α-FeOOH	Photocatalysis-photo-Fenton	Sunlight	tetracycline	94% removal in 60 min	Oxidation at different pH values; Removal drastically higher than in separate processes	Less H_2O_2 consumption, but necessary for oxidation; stability decreases after 5th cycle	[101]
TiO_2-graphene oxide-Fe_3O_4	Photocatalysis-photo-Fenton	Visible light	Amoxicillin antibiotic	90% TOC pH = 3 50% TOC pH = 5 in 120 min	Magnetic recovery properties	TOC degradation is kept constant until 5th run; leached iron detected in all runs (<1 mg/L)	[102]
Fe-Cu oxide/diamond	Photocatalysis-photo-Fenton	Visible light	Phenol	100% phenol removal in 120 min pH = 4	Iron and copper cycle involved in Fenton reactions	Not good reusability; Expensive support	[103]
$Zn_{1-1.5x}Fe_xS$/ g-C_3N_4	Photocatalysis-photo-Fenton	Visible light	p-nitrophenol	96% removal and 55% TOC in 60 min	Incorporation of Fe in crystal lattice improves degradation rates	Not photocatalytic contribution; Ow reusability of the catalysts	[109]
$FeTiO_3$	Photocatalysis-photo-Fenton	Solar light, visible light	Phenol and sulfon-amides	100% removal and 98% mineralization	Synergy between processes; low cost of catalyst.	Small iron concentration leached	[104,111,112]
$FeTiO_3$	Photocatalysis-photo-Fenton	UV–Vis; high tem-perature	Real hospital wastewater	80% TOC in 300 min	Synergy between processes; low cost of catalyst	Small iron concentration leached	[113]
$La_{1-x}Ti_xFeO_3$	Photocatalysis-photo-Fenton	UV, solar and visible light	4-Cl-phenol	100% and 100% mineralization in 120 min	One single-phase catalyst; the substitution lattice improved redox properties	No iron detected	[107,108,114]
Graphene/ Fe_3O_4	Photocatalysis-photo-Fenton	UV light	Methyl orange	99% removal of dye	Synergy with respect to Fe_3O_4	Slight decrease in activity	[105]

Table 8. Photocatalysts employed for persulfate activation.

Catalyst	Processes	Conditions	Pollutant	Yield	Advantages	Disadvantages	Ref.
TiO_2/g-C_3N_4	PS/photocatalysis	Vis light	Acetaminophen	100% removal in 30 min 86% TOC in 60 min	Persulfate got 13 times activity than single photocatalyst	Reduction of 5 percent of activity after 5 cycles	[81]
ZnO	PS/photocatalysis	Sunlight	Pesticides	92% TOC in 1000 min	Improvement reaction rate	Generation of big loads of sulphate in solution	[115]
Ag/AgBr/ $ZnFe_2O_4$	PS/photocatalysis	Visible light	Carbamazepine	53% removal; double of activity with PS.	LED light; magnetic separation	When using H_2O_2 the Z-scheme was inhibited and a reduction of the degradation	[116]
Co-doped $Bi_2Fe_4O_9$	PS/photocatalysis	Visible light	Levofloxacin		LED light; doped materials have 3.52 times higher than that non-doped;	Iron and cobalt leaching	[117]
Ilmenite	PS/photocatalysis	UV light	Azo dye	>95% of mineralization	improvement reaction rate; no iron leached	Generation of big loads of sulphate in solution	[118]

4. Catalyst Immobilisation: Intensification of Reactor Design

Some of the main previous strategies have also been gathered into a further step for implementation of the photocatalytic process in a continuous mode, which inherently involves the immobilisation of the photoactive material onto solid media. In addition, immobilisation provokes a reduction of energy investment by a decrease in the number of process units. Globally, the support media must integrate some characteristics: (i) to allow high light transmission, (ii) to possess chemical and mechanical stability, and (iii) to have the ability to keep the solid photocatalyst attached to the surface during photoreactions [119].

Until now, there have been two kinds of supports that solve the problem of handling powdery catalysts and make catalyst replacement easier once the reaction is performed. Those are the multichannel monoliths and the open-cell alveolar ceramic foams. In the case of monoliths, they are the substitute of the packed-bed photocatalyst, but they suffer from poor light transmission in their inner parts and do not allow the photoreaction to proceed. While in the case of open-cell alveolar foams, they benefit from acting as a static mixer, which can work under low pressure drop, and they have higher light transmission on the entire surface. For them, works dealing with (β-)SiC, ZrO_2 and metallic foams for attaching the photocatalyst have been reported. In this context, the main studies that report the use of media for photo-assisted wastewater photo-assisted treatment can be seen in Table 9.

Most works are devoted to a pure photocatalytic process in which titania is the supported photocatalyst par excellence [120–123], while only two works have been found in the literature dealing with the photo-Fenton process involving iron-based materials anchoring in a medium [124,125]. It must be highlighted that the works of Rico-Santacruz et al. [122,123] are not characterised by the attachment of the catalyst to the support unless by the one-step synthesis of the whole active phase/support, avoiding in this manner, the leaching of the active phase to the liquid solution. Some details are found in Table 9.

Table 9. Photocatalysts immobilised onto supports for water treatment of AOPs.

Catalyst/ Support	Conditions	Advantages	Disadvantages	Ref.
TiO_2/β-SiC	Pesticide pyrimethanil /photocatalysis	Titania coating optimized; no active phase release		[121]
TiO_2/β-SiC	Nanoplastic pollutants /photocatalysis	Titania coating optimized; no active phase release		[120]
TiO_2/ZrO_2	CEC and disinfection /photocatalysis		No evaluation of active phase release	[126]
TiO_2@β-SiC	Diuron pesticide /photocatalysis	Single unique phase; no separation between the active phase and the support.	No active phase release	[122,123]
Perovskite/ monolith	Methylparaben /photo-Fenton	Photo-Fenton at $pH_0 = 7$		[125]
TiO_2-$FeSO_4$/ metallic foam	Malachite green dye/photo-Fenton	LED employment	Small amount of Fe leached	[124]

5. Process Combination

This section offers investigations that reported the combination of processes, either because of a combination of different photo-assisted advanced oxidation processes (AOPs) or because of a combination of at least one AOP with another type of treatment. In the same way, this section will review and classify the combined treatments as those that are hybrid or single-step processes and sequential or two-step processes, as seen in Figure 6.

During the latest years, the scientific community has focused on the study of technologies combination. However, most of these studies have been performed at the lab scale, with very low implementation on a pilot and real scale. Therefore, this section especially summarises the recent advances at the lab scale by combining technologies.

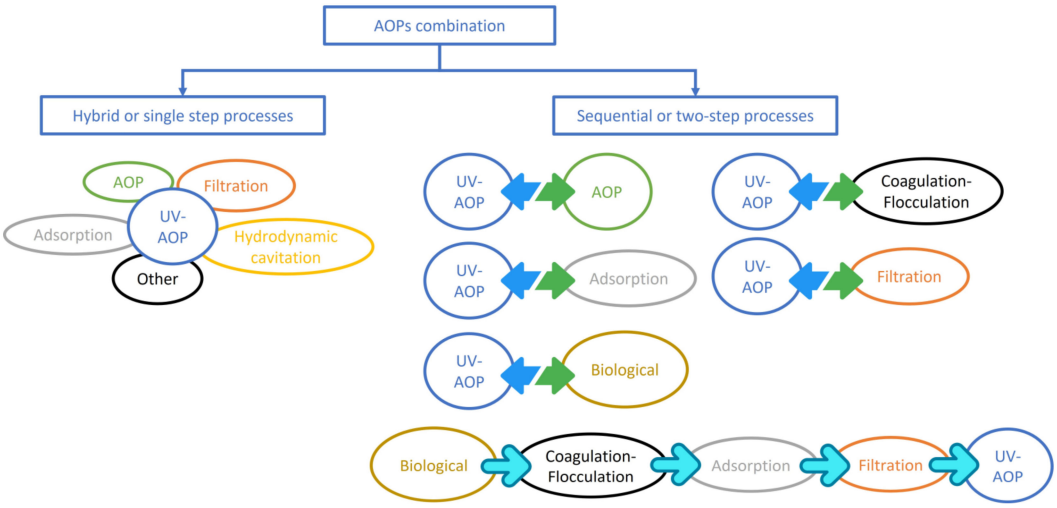

Figure 6. Possibilities of combining UV-AOPs in a single or sequenced stage.

In this way, the combination of processes only has one objective: increasing the treatment capacity of the process, either by an accumulative effect as a consequence of the increase in the production of free radical species, or by a synergistic effect by the positive interaction of the individual processes [127]. The calculation of the synergistic effect has been reported by different authors in different ways. While Dewil et al. [127] reported the calculation following Equation (7), Spuhler et al. [128] followed Equation (8).

$$S = \frac{k_{combined} - \sum_1^n k_i}{k_{combined}} \tag{7}$$

$$S = \frac{k_{combined}}{\sum_i^n k_i} \tag{8}$$

It seems logical to think that a combination of treatments is carried out with the aim of obtaining a positive synergetic effect. However, this does not always happen, and sometimes, this combination does not necessarily have to be beneficial from the point of view of final performance. This effect may be more common when the combination of processes involves different AOPs and is a consequence of the excess of radical species generated, which can produce scavenger effects.

5.1. Hybrid/Integrated Systems including at Least One Photo-Assisted AOP

Therefore, in a first approach, we will describe the recent literature found about the combination processes as a hybrid or integrated system. Most of the research has been focused separately on photo-assisted advanced oxidation processes. However, hybrid or integrated systems are single-step processes that use the advantages of available treatment to overcome the challenges and limitations during the removal of pollutants. These hybrid systems can be divided by a combination of a photo-assisted AOP with other AOPs or with other kinds of technologies (physical, chemical, or biological).

Table 10 summarises a collection of recent hybrid treatments based on the combination of a photo-assisted AOP with other AOPs in a single step. Furthermore, in these combinations, the authors have proved the synergistic effect as a result of combination of two AOPs in a single step with respect to the effect of the different AOPs individually.

Table 10. Hybrid or single-step combination of photo-assisted advanced oxidation processes.

Combination	Target Pollutant	Water Matrix	Maximum Efficiency	Remarks	Ref.
O_3/H_2O_2/ UV-C ZnO/$Na_2S_2O_8$/ UV-C $TiO_2/Na_2S_2O_8$/ UV-C	Fluroxypyr and Triclopyr (herbicides)	Drinking water (DW) Leaching water (LW)	92% Fluroxypyr in DW; 62% Triclopyr in DW, reached with O_3/H_2O_2/UV-C system (120 min)	H_2O_2 = 75 mg/L; O_3 = 500 mg/h; pH = 7.3 (LW); 8.2 (DW) ZnO = 300 mg/L; $Na_2S_2O_2$ = 300 mg/L; pH = 7.3 (LW); 8.2 (DW) TiO_2 = 300 mg/L; $Na_2S_2O_2$ = 300 mg/L; pH = 7.3 (LW); 8.2 (DW)	[129]
O_3/H_2O_2/ UV-A	Sulfamethoxazole (antibiotic)	Ultrapure water (UW)	100% (15 min)	H_2O_2 = 45.3 µL; O_3 = 50g/m^3; pH = 5.1	[130]
O_3/H_2O_2/ UV-A	Methylparaben, ethylparaben, propylparaben, butylparaben and benzylparaben (parabens)	Ultrapure water (UW)	100% (90 min)	H_2O_2 = 13.5 mg/L; O_3 = 0.2 mg/L; pH = 5.7	[131]
Solar Photo-Fenton/O_3	Acetaminophen (drug), antipyrine (analgesic), bisphenol A (additive), caffeine (drug abuse), metoprolol (β-blocker) and testosterone (hormone)	Milli-Q water (UW)	≈100% in average (10 min)	Fe(III) = 2.79 mg/L; H_2O_2/Fe(III) = 6.09 (mass); average incident UV-A solar radiation 41.2 W/m^2; O_3 = 13 mg/L; pH = 3	[132]
TiO_2/Solar radiation/O_3			≈100% in average (15–20 min)	TiO_2 = 200 mg/L; average incident UV-A solar radiation 41.2 W/m^2; Ozone = 13 mg/L; pH = 7	
Solar photo-Fenton/O_3 Solar H_2O_2/O_3 Solar Fe/O_3	Pentachlorophenol (plaguicide), Terbutryn (herbicide), Chlorofenvinphos (insecticide), Diclofenac (drug)	Ultrapure water (UW) Natural water (NW) Simulated wastewater (SW)	80% in average (4.4 kJ/L) in SW	H_2O_2 = 1.5 mM; Fe(II) and Fe(III) = 0.1 mM; O_3 = 0.2–0.6 mg/L; pH = 8	[133]
Solar TiO_2/O_3	DEET (insecticide)	Ultrapure water (UW) Real Wastewater (WW)	≈90% (10 min)	TiO_2 = 150 g/L (supported); pH = 8; O_3 = 15 mg/L; I_{solar} =550 W/m^2	[134]
$TiO_2/UV/O_3$	Dimethyl silanediol, acetic acid; diisobutyl phthalate (odour compounds)	Industrial wastewater (IW)	63.8% Dimethyl silanediol; 41.5% acetic acid; 74.2% diisobutyl phthalate (25 min)	O_3 = 16 mg/L; pH = 7.5; TiO_2 = 3 g/L	[135]
TiO_2/O_3/UV-A	Methyl-dopa and famotidine (drugs), and nalidixic acid (antibiotic)	Ultrapure water (UW)	84.93–99.15% (30 min)	O_3 = 6 L/h; TiO_2 (supported) = 12.5 g/L	[136]
$TiO_2/UV/O_3/H_2O_2$	Volatile Organic Compounds mix	Simulated wastewater	98% (30 min)	TiO_2 = 100 mg/L; O_3 = 5.92 g; H_2O_2 = 1.78 g	[137]
PMS/TiO_2/ UV-A	Methylene Blue (dye)	Ultrapure water (UW)	>90% (60 min)	PMS = 0.32 mM; TiO_2 = 5 mM; pH = 7	[138]
Solar photo-Fenton/TiO_2	Metronidazole (antibiotic)	Real Wastewater (WW)	≈60% (15 min)	H_2O_2 = 450 mg/L; pH = 3.0–3.5; Fe and TiO_2 supported	[139]
Solar photoelectron-Fenton (Fe_3O_4/ ZnO/graphene)	Pyrimethanil and Methomyl mix (pesticides)	Ultrapure water (UW)	>50% (5 min)	Na_2SO_4 = 50 mM; pH = 3.0; j = 74 mA/cm^2; Q = 5.6 L/min; Q_{air} = 10 L/min; Fe(II) = 0.5 mM; 64.9 mg H_2O_2/min	[140]
Sono photo-Fenton	Methylene blue and Congo red (dyes)	Ultrapure water (UW)	100% (<60 min)	40 W UV-C lamps; 40 kHz of US; Fe_3O_4/ZnO/graphene nanocomposites; Ph = 3 and 13; H_2O_2 = 4 mL	[141]
Sono photo-Fenton	Di-n-butyl phthalate (plasticizer)	Ultrapure water (UW)	80% (30 min)	Fe(II) = 0.1 mM; 400 kHz; UV-C; pH = 2–9; H_2O_2 = 0.025–0.2 mM	[142]
CuO_x–$BiVO_4$/SPS/ Solar System	Sulfamethoxazole	Ultrapure water (UW), bottled water (BW) secondary wastewater (WW)	UW: 100% (30 min) BW: 100% (60 min) WW: 60% (120 min)	Solar radiation; [SPS] = 500 mg/L; [Catalyst] = 500 mg/L; 0.75, 3.0 and 10.0 Cu.BVO	[143]
CoAl-LDH/ BiOBr/PMS/ Visible	Ciprofloxacin	Ultrapure water (UW)	96% (30 min)	300 W Xenon lamp; 8wt% CoAl-LDH-BiOBr; [PMS] = 60–100 mg/L; [Catalyst] = 30–50 mg/L	[144]
WO_3/BiOBr/ PMS/visible	Tetracycline and enrofloxacin	Ultrapure water (UW)	Tetracycline: 98% (60 min) Enrofloxacin: 87%	300 W Xenon lamp; 2 WO_3 + BiOBr; [PMS] = 30 mg/L; [Catalyst] = 20–60 mg	[145]
PDS/H_2O_2/Fe/ Solar radiation	*E. coli* (bacteria); MS2 (bacteriophage); 13 micropollutants mix	Ultrapure water (UW)	>6-Log for *E. coli* (30 min) and MS2 (10 min); >90% for micropollutants (30 min)	H_2O_2 = 10 ppm; 40°CM Fe(II) = 1 ppm; PDS = 9 × 10^{-5} M; 900 W/m^2	[146]
PMS/H_2O_2/Fe/ Solar radiation	*E. coli* (bacteria) 13 micropollutants mix	Natural water (NW)	>6-Log for *E. coli* (20 min); >90% for micropollutants (15 min)	H_2O_2 = 10 ppm; 40°CM Fe(II) = 1 ppm; PMS = 3.6 × 10^{-5} M; 900 W/m^2	[147]

As can be observed in Table 10, there are many references exploring this combination of photo-assisted AOPs. In general, the combination comes from the mix of oxidants (O_3, H_2O_2, peroxymonosulfate (PMS) or peroxydisulfate (PDS), etc.) with catalysts (TiO_2, ZnO, Fe_3O_4 or other iron species, etc.) in the presence of different kinds of UV radiation (UV-C, UV-A, UV–Vis, solar radiation), or combined with electro or sono- AOPs. Although there is no clear trend, since for this combination of processes, researchers apply it both to the elimination of pathogens [146,147] and to the removal of micropollutants [129–136,138–142], most of the work focusses on the latter. When micropollutants are used as a target pollutant to test the synergy of the treatments, these are normally tested in ultrapure water matrices [130–134,136,138,140–142,146] with a very low influence of other substances present in water, ensuring very high performance (between 90 and 100% of removal), while when more complex aqueous matrices are used, such as natural water or real or simulated urban or industrial wastewater [129,133–135,137,139,147], the performance is lower or a higher reaction time is required to reach total removal. Most of these works are performed on a laboratory scale. The main reason is that AOPs are still emerging technologies without the maturity level necessary to be implemented on a full scale, and this coupling of AOPs in hybrid systems is one more step in the maturation process of this technology.

Therefore, it is worth highlighting the work carried out on complex water samples. For example, Pérez-Lucas et al. [129] studied the combination of different photo-assisted AOPs in a single step (O_3/H_2O_2/UV-C; $ZnO/Na_2S_2O_8$/UV-C and $TiO_2/Na_2S_2O_8$/UV-C) on the removal of two different herbicides (Fluroxypyr and Triclopyr) present in natural and leaching water. Under these operating conditions, 92 and 62% of removal of fluroxypyr and Triclopyr, respectively, was obtained after 120 min, being reduced to 66 and 13% in leaching water samples due to the complexity of these samples. Roccamante et al. [133] studied the removal of a mixture of four different micropollutants (Pentachlorophenol, Terbutryn, Chlorofenvinphos and Diclofenac) in different water matrices (simulated, natural and simulated wastewater) using solar-driven AOP (solar photo-Fenton, solar H_2O_2 and solar Fe(II)) in combination with ozonation. Under these operating conditions, Roccamante et al. reported an average removal of the mixture of micropollutants of 80% with an accumulated dose of radiation of 4 kJ/L when the treatments were applied over the simulated wastewater sample, which is the most complex sample of the three studied. Talwar et al. [139] described a 60% metronidazole after 15 min of treatment using a combination of solar photo-Fenton applied in a cylindrical parabolic collector (CPC) together with TiO_2 as a photocatalyst. Moving to another field of application, Rodríguez-Chueca et al. [147] reported the simultaneous removal of microorganisms and 13 micropollutants with the PMS/solar photo-Fenton system in natural water samples. In this work, the total removal of *E. coli* was observed in 20 min of reaction, while 15 min was required to reduce the average concentration of more than 90% of the 13 micropollutants.

On the other hand, Table 11 summarises the combination of photo-assisted AOPs with other kind of technologies.

In this case, as observed in Table 10, different physical or chemical technologies are the most adequate to pair in the same step with these AOPs, especially the filtration steps, such as microfiltration, ultrafiltration or nanofiltration [148–150], adsorption with activated carbon [151] or hydrodynamic cavitation [152]. The combination of photo-assisted AOPs with a filtration system is particularly noteworthy. The maturity level of this system can be considered higher than the hybrid combination of AOPs shown in Table 10, especially in well-known photocatalytic membrane reactors or, in other words, in photocatalytic membrane reactors. This higher level of maturity is demonstrated in the greater application of these technologies over complex water matrices, such as simulated or real wastewater samples.

Table 11. Hybrid or single-step combination photo-assisted advanced oxidation processes with other technologies.

Combination	Target Pollutant	Water Matrix	Maximum Efficiency	Remarks	Ref.
TiO_2/UV-C/Microfiltration	*E. coli* (bacteria), *Enterococcus* sp. (bacteria), *Candida albicans* (fungi)	Simulated wastewater (SW)	4-Log	316-L porous stainless-steel membranes; 0.2 gTiO_2/membrane; UV-C (254 nm)	[148]
Photo-Fenton/ Ultrafiltration	Chemical Oxygen Demand (COD); Total Organic Carbon (TOC)	Industrial wastewater (IW)	85.9% COD; 74.5% TOC	Under UV-A: pH = 4.00; H_2O_2/Fe^{2+} (g/g) = 10.75 Under UV-C: pH = 4.44; H_2O_2/Fe^{2+} (g/g) = 7.27	[149]
TiO_2/UV/ Ultrafiltration	Chemical Oxygen Demand (COD); Total Organic Carbon (TOC)	Industrial wastewater (IW)	87.4% COD; 70% TOC (360 min)	UV-A (340 nm); 10 g TiO_2 immobilized to Halloysite nanotubes; Hollow fibre ultrafiltration membrane	[150]
Activated Carbon/US/UV/ H_2O_2	Chemical Oxygen Demand (COD)	Petrochemical wastewater (IW)	87% (80 min)	pH = 4.0 ± 0.2; Activated Carbon = 0.4 g/L; H_2O_2 8.0 mM; 320 W US	[151]
Hydrodynamic cavitation/photo-Fenton	Imidacloprid (insecticide)	Ultrapure water (DW)	99.23% (15 min)	H_2O_2 = 3.91 mM; Fe(II):H_2O_2 = 1:40; UV-A (364 nm); inlet pressure from 5 to 20 bar	[152]
Hydrodynamic cavitation/UV-A			45.56% (120 min)	UV-A (364 nm); inlet pressure from 5 to 20 bar	
Hydrodynamic cavitation/photocatalysis			55.18% (120 min)	Nb_2O_5 = 200 mg/L; UV-A (364 nm); inlet pressure from 5 to 20 bar	

Rodríguez-Chueca et al. [148] reduced the microbial population in simulated wastewater samples using a photocatalytic membrane reactor, combining TiO_2 with UV-C radiation and microfiltration. Under the reported operating conditions, 4-log units of *E. coli*, *Enterococcus* sp., and *Candida albicans* were reduced in simulated wastewater samples using a very short contact time. In a photocatalytic membrane reactor, Moslehyani et al. [150] reported the successful reduction in organic matter content in terms of COD and TOC (87.4 and 70%, respectively) in industrial wastewater, using ultrafiltration and TiO_2 exposed to UV-A radiation. Similar to photocatalytic membrane reactors but working in a homogeneous phase, the combined system proposed by Aydiner et al. [149], in which photo-Fenton (with UV-A or UV-C radiation) was combined with ultrafiltration to reduce the content of organic matter (COD and TOC) in industrial wastewater samples, reached similar results to the reported by Moslehyani et al. with TiO_2 [150]. In the same level of reduction of the organic matter content (87% of COD) in industrial wastewater are the results reported by Kakavandi and Ahmadi [151]; however, in this case, photo-assisted AOP was not combined with a filtration step, but also, a combination of activated carbon with sonication and H_2O_2/UV was used. Therefore, in general terms, it is clearly observed that hybrid systems combining AOPs with other technologies have proven to be mature enough to reduce organic content and organic micropollutants in complex water matrices, demonstrating the synergistic effect caused by the different treatments performed by separation.

5.2. Sequential or Two-Step Combination Processes

Not always is the combination of processes in a single step technically possible; even this combination should be the best one in terms of efficiency. For this reason, the combination of processes in sequential or two-step systems is also studied. This is also called a treatment chain or treatment train.

In the first approach, this section summarises those research reports where treatment trains combine different AOPs (with at least one photo-assisted). This information is shown in Table 12.

Table 12. Sequential or two-step combination of advanced oxidation processes.

Combination	Target Pollutant	Water Matrix	Efficiency	Remarks	Ref.
Ozonation/UV/ H_2O_2	N,N-Diethyl-p-phenylenediamine sulfate, nitrobenzene, benzoic acid	Ultrapure water (UW) with Dissolved Organic Matter	Benzoic acid 80% (30 min)	O_3 = 5 mg/L; UV-C (254 nm); H_2O_2 = 1 mM; pH = 7	[153]
Ozonation/UV/ $S_2O_8^{2-}$			Benzoic acid > 90% (30 min)	O_3 = 5 mg/L; UV-C (254 nm); $S_2O_8^{2-}$ = 1 mM; pH = 7	
Ozonation/UV/ HClO			Benzoic acid > 20% (20 min)	O_3 = 5 mg/L UV-C (254 nm); HClO = 5 mg/L; pH = 7	
Electrocoagulation/ Electrooxidation/ PMS/UV/$CuFe_2O_4$	Chemical Oxygen Demand (COD); Total Organic Carbon (TOC); Biochemical Oxygen Demand (BOD), Ammonia (NH_4^+)	Landfill leachate (LL)	COD 95.6%; TOC 90.5%; BOD 91.6%; NH_4^+ 99.8%	Current density = 50 mA/cm^2; PbO_2 anode; pH = 5; PMS = 15 mM; $CuFe_2O_4$ = 0.15 g/L	[154]

As can be seen in Table 10, the sequential combination of AOPs is not common in the literature. It is not clear, the reason to explain this, except to think that AOPs are such efficient treatments from a contaminant removal point of view, it does not seem to make much sense to combine more than one treatment in sequence. Normally, the combination of treatments in sequence aims to remove contaminants of a different nature (organic, inorganic, metals, microorganisms, etc.), and therefore, treatments of a different nature are used. However, the use of AOPs is exclusively focused on the chemical oxidation of organic and biological contaminants; thus, if these are reduced in great quantities in a first stage, it does not seem to make much sense to include a new subsequent stage with the same nature. However, Sun et al. [153] reported the removal of N,N-Diethyl-p- phenylenediamine sulphate, nitrobenzene and benzoic acid through a sequential combination of ozonation and different photo-assisted AOPs (such as H_2O_2/UV, $S_2O_8^{2-}$/UV and HClO/UV). Under the operating conditions reported by Sun et al. [153], acid benzoic was reduced by more than 90% in the $O_3/S_2O_8^{2-}$/UV system, followed by O_3/H_2O_2/UV with a yield of 80%. Ghanbari et al. [154] reported a reduction in organic matter in more than 90% (COD and TOC) in landfill leachate by sequential combination of electrocoagulation/electrooxidation and the $CuFe_2O_4$/PMS/UV system.

In addition, as mentioned above, it makes more sense to combine, in sequence, AOPs with other different technologies, in order to reach synergies and to maximise the removal of pollutants in water. In addition, AOPs are always considered the last step in a chain treatment because of their ability to remove organic micropollutants or pathogenic germs, and because the cleaner the water matrix, the more effective it is. Therefore, these AOPs may be coupled with biological treatments in order to reduce previously the content of organic matter, such as with coagulation–flocculation to reduce the colloidal matter in water, with adsorption, or with filtration systems to maximise the removal of a certain organic substance or a group of them. Table 13 summarises recent references in the literature studying this treatment train that include at least one photo-assisted AOP. These treatment trains are more focused on the treatment of real water samples, especially focused on the treatment of industrial or urban wastewater, and at a larger scale than those treatments shown in the previous tables.

Table 13. Sequential or two-step combination processes (one photo-assisted AOP + other technology).

Combination	Target Pollutant	Water Matrix	Efficiency	Remarks	Ref.
Biological/ Coagulation–flocculation/Photo-Fenton/Biological	Chemical Oxygen Demand (COD); Biochemical Oxygen Demand (BOD); Ammonium; Alkalinity; chromium; total suspended solids (TSS); recalcitrant organic compounds	Leather tannery landfill leachate (LL)	The efficiency for each target pollutant is not reported in the global system	Continuous-flow SBR: 2.0 g/L < MLVSS < 4.0 g/L; sludge volume index (SVI) of 53 mL/g; 200–400 mg/L $FeCl_3$ as coagulant at pH 3; H_2O_2 = 400 mg/L; Dissolved iron = 150 mg/L	[155]
Biological/ Coagulation–flocculation/Photo-electroFenton/ Biological				Continuous-flow SBR: 2.0 g/L < MLVSS < 4.0 g/L; sludge volume index (SVI) of 53 mL/g; 200–400 mg/L $FeCl_3$ as coagulant at pH 3; H_2O_2 = 400 mg/L; Dissolved iron = 150 mg/L; Current density = 300 mA/cm^2	
Solar photo-Fenton/Activated sludge	Chemical Oxygen Demand (COD); Total Organic Carbon (TOC)	Low strength Industrial wastewater (IW)	84% (COD)	pH = 3; H_2O_2 = 0.25 M; Fe(II) = 0.05 M; 20% (v/v) sludge concentration	[156]
		High strength Industrial wastewater (IW)	82% (COD)	pH = 3; H_2O_2 = 1 M; Fe(II) = 0.1 M; 25% (v/v) sludge concentration	
Electrocoagulation/ Adsorption/photo-Fenton-like	Chemical Oxygen Demand (COD); Total Organic Carbon (TOC); Turbidity; Colour; Suspended Solids (SS)	Textile Wastewater (IW)	87% (TOC); 49% (COD); 96% (Turbidity); 90% (Colour); 95–97% (SS)	Electrocoagulation: Al Electrode; current density = 25 mA/cm^2; pH = 5. Adsorption: 1 g/L corncob. Photo-Fenton-like: $BiNiO_3$ = 0.75 g/L; H_2O_2 = 2–8 mM; pH = 7–7.5	[157]
Activated sludge/H_2O_2/ UV-C	Carbamazepine; Clarithromycin; Diclofenac; Metoprolol; Benzotriazole; Mecoprop.	Urban Wastewater (WW)	Average removal micropollutants: 25% (activated sludge) + 100% (10 min)	Activated sludge: hydraulic retention time = 4 h; sludge retention time = 2 d; H_2O_2 = 25 mg/L	[158]
Activated sludge/solar photo-Fenton			Average removal micropollutants: 25% (activated sludge) + 28% (60 min)	Activated sludge: hydraulic retention time = 4 h; sludge retention time = 2 d Fe(II) = 5 mg/L; H_2O_2 = 25 mg/L	
Moving bed bioreactor/H_2O_2/ UV-C			Average removal micropollutants: 40% (moving bed bioreactor) + 100% (10 min)	Moving bed bioreactor: no remarks; H_2O_2 = 25 mg/L	
Moving bed bioreactor/solar photo-Fenton			Average removal micropollutants: 40% (moving bed bioreactor) + 31% (60 min)	Moving bed bioreactor: no remarks; Fe(II) = 5 mg/L; H_2O_2 = 25 mg/L	
Coagulation–Flocculation/H_2O_2/ UV-C			Average removal micropollutants: 20% (coagulation–flocculation) + 100% (30 min)	Coagulation–flocculation = $FeCl_3$ (40%) as coagulant. H_2O_2 = 25 mg/L	
Coagulation–Flocculation/solar photo-Fenton			Average removal micropollutants: 20% (coagulation–flocculation) + 11% (60 min)	Coagulation–flocculation = $FeCl_3$ (40%) as coagulant. Fe(II) = 5 mg/L; H_2O_2 = 25 mg/L	

Table 13. *Cont.*

Combination	Target Pollutant	Water Matrix	Efficiency	Remarks	Ref.
TiO_2/UV/ Ultrafiltration	Dissolved Organic Carbon (DOC)	Simulated fresh water	>80% (120 min)	10 kDa-flat sheet polyethersulfone (PES) membrane 41.8 cm^2; TiO_2 = 0.4–0–6 g/L; UV-A (354 nm)	[159]
O_3/H_2O_2/Carbon based biofilter/ UV-C/H_2O_2	13 detected micropollutants	Treated real wastewater (WW)	O_3/H_2O_2 = 78%; Carbon based biofilter = 87%; UV/H_2O_2 = 43%	O_3 = 13 ± 0.5 mg/L, H_2O_2 = 11 ± 0.4 mg/L for the O_3/H_2O_2 process, and UV = 410 ± 63.5 mJ/cm^2, H_2O_2 = 5 mg/L for the UV-C/H_2O_2 process	[160]
O_3/H_2O_2/ Limestone Based Biofilter/UV-C/H_2O_2			O_3/H_2O_2 = 78%; Limestone based biofilter = 67%; UV/H_2O_2 = 43%		
O_3/H_2O_2/ Ultrafiltration/ UV-C/H_2O_2/ Reverse Osmosis			O_3/H_2O_2 = 78%; Ultrafiltration = 0%; UV/H_2O_2 = 43%; Reverse osmosis = 99%		
Coagulation–flocculation/ solar photo-Fenton/aerobic bio-treatment	Chemical Oxygen Demand (COD); Dissolved Organic Carbon (DOC); Total polyphenol content (TPC)	Cork boiling wastewater (IW)	Coagulation–flocculation/solar photo-Fenton = 93,4% (COD); 92,8% (DOC); 94,5% (TPC)	Coagulation–flocculation: $FeCl_3$ as coagulant (3 min 100 rpm + 30 min 30 rpm + 30 min). Solar photo-Fenton: Fe(III) from coagulation = 46–80 mg/L; H_2O_2 = 1–2.5 g/L; Sequencing Batch Bioreactor (Activated sludge)	[161]
Moving bed bioreactor/ photo-Fenton	Chemical Oxygen Demand (COD); Total Organic Carbon (TOC); Oil and grease	Industrial Wastewater (IW)	>95% (COD)	Fe(II):H_2O_2 = 250:800 (mg/L)	[162]
Coagulation–flocculation/ UV-A-LED/ Photo-Fenton	Chemical Oxygen Demand (COD)	Industrial wastewater (IW)	74% (360 min)	H_2O_2 = 5459 mg/L; Fe(III) = 286 mg/L; UV-A LED 85 W/m^2	[163]
Photo-Fenton/ Chemical Addition Dissolved Air Flotation (CA-DAF)	Chemical Oxygen Demand (COD); Total Petroleum Hydrocarbon (TPH)	Industrial wastewater (IW)	99.85% for COD and 98.9% for TPH	pH = 3; $FeSO_4$ = 100 mg/L; H_2O_2 = 17.8 g/L. For DAF unit volume and loading rate were 7 m^3 and 35–40 L/min. Aeration rate 15–20 L/min, and pressure was set at 3 bar and the saturation time of 30 min	[164]
Coagulation–flocculation/ Photo-Fenton	*E. coli*; *Enterococcus* sp.; *Pseudomonas aeruginosa*	Simulated wastewater (SW)	>4 log in all bacteria (210 min)	pH = 5; Fe(III) = 5 mg/L; H_2O_2 = 25 mg/L	[165]
Coagulation–Flocculation/ H_2O_2/UV-C	Detected micropollutants	Treated urban wastewater (WW)	Average removal: Coagulation–flocculation < 10%; 55% (H_2O_2/UV-C)	Coagulation–flocculation = 1.1 kg/m^3 of polyelectrolyte; H_2O_2 = 0.5 mM; pH = natural	[166]
Coagulation–Flocculation/ PDS/UV-C			Average removal: Coagulation–flocculation < 10%; <20% (PDS/UV-C)	Coagulation–flocculation = 1.1 kg/m^3 of polyelectrolyte; PDS = 0.5 mM; pH = natural	
Coagulation–Flocculation/ PMS/UV-C			Average removal: Coagulation–flocculation < 10%; 48% (H_2O_2/UV-C)	Coagulation–flocculation = 1.1 kg/m^3 of polyelectrolyte; PMS = 0.5 mM; pH = natural	

As it has been previously mentioned and as seen in Table 13, these treatment trains are normally tested over real water samples, especially over samples with a higher complexity such as urban and industrial wastewater, due to the combination of mature technology (biological, coagulation–flocculation, adsorption or filtration systems) with an emerging technique such as AOPs. In addition, in this case, research is focused not only on the removal of emerging pollutants but also on the reduction of organic matter content or other parameters usually controlled for in regular wastewater treatment facilities, such as nitrogen, phosphorus, turbidity, total suspended solids, or even microorganisms. The works presented in Table 13 are not comparable with each other when analysing different water matrices, with different operating conditions, even with different types of unitary processes within the treatment chain. However, it can be concluded that the combination of processes is what increases the results of the elimination of the pollutants in question.

6. Concluding Remarks

In conclusion, UV-AOPs have been successfully applied to the removal of a wide range of contaminants from polluted water. However, their application at an industrial scale remains a challenge due to the high operational costs associated with these processes. To address this issue, intensifying UV-AOPs through optimisation of operating conditions and development of bifunctional catalysts is a promising approach for improving their feasibility and effectiveness on an industrial scale.

Recent research has focused on optimising different operational parameters, such as catalyst loading, pH, temperature, and oxidant concentration, to augment the photocatalytic process efficiency and reduce reagent consumption and treatment time. The efficiency of UV-AOPs is sensitive to these parameters, and while increasing catalyst loading can improve pollutant removal rates, exceeding the maximum optimal value can slow the rate of mineralisation. Different studies have found varying optimal concentrations for different catalysts and conditions, and some have developed models to better understand the dependence of reaction rates on catalyst loadings.

The review also discusses the development of photocatalytic materials for intensifying the UV-AOPs process. This optimisation has primarily been in two directions: to reduce the physical limitations of the reaction and to increase the overall yield of the treatment, which is also related to the chemical limitations. The main approaches to intensifying photocatalysts can be divided into two main categories: design orientated to reduce mass and photon transfer limitations and design of bifunctional catalysts that increase the generation of oxidising species. These strategies are further discussed, including the main approaches found in the literature for each of them.

Additionally, the review examines the combination of different photo-assisted AOPs for the treatment of pollutants. The combination of processes is often carried out with the aim of achieving a positive synergistic effect, but this is not always the case. The text also describes hybrid and integrated systems that combine AOPs with other technologies and reports on recent research in this area. However, while much research has been on AOPs on the laboratory scale, there has been little implementation on pilot or real scales. Therefore, more research is needed to better understand the mechanisms of these combinations and to improve their applicability at larger scales.

In conclusion, intensifying UV-AOPs through optimisation of operating conditions and development of bifunctional catalysts are promising approaches for improving their feasibility and effectiveness on an industrial scale. Further research is also necessary to better understand the mechanisms of combining different photo-assisted AOPs and to improve their applicability at larger scales.

Author Contributions: Conceptualization, J.R.-C., J.C. and P.G.-M.; methodology, J.R.-C., J.C. and P.G.-M.; formal analysis, J.R.-C., J.C. and P.G.-M.; investigation, J.R.-C., J.C. and P.G.-M.; writing—original draft preparation, J.R.-C., J.C. and P.G.-M.; writing—review and editing, J.R.-C., J.C. and P.G.-M.; visualization, J.R.-C., J.C. and P.G.-M. All authors have equally contributed to this manuscript. All authors have read and agreed to the published version of the manuscript.

Funding: J.R.-C. acknowledges Comunidad de Madrid for funding by the pluriannual agreement with the Polytechnic University of Madrid in the line of action Programme of Excellence for University Teaching Staff (M190020074BJJRC). P.G.-M. acknowledges Comunidad de Madrid through the call Research Grants for Young Investigators from Universidad Politécnica de Madrid for funding the research project SUNCAT4PLAST (APOYO-JOVENES-21-JV4DEB-3-Q2WGKV). J.R.-C. and P.G.-M. acknowledge the Spanish Ministry of Science and Innovation for funding the research project PHOTORAS (PID2021-128165OA-I00).

Informed Consent Statement: Not Applicable.

Data Availability Statement: Data sharing is not applicable to this article.

Conflicts of Interest: The authors declare no conflict of interest.

References

1. Pandis, P.K.; Kalogirou, C.; Kanellou, E.; Vaitsis, C.; Savvidou, M.G.; Sourkouni, G.; Zorpas, A.A.; Argirusis, C. Key Points of Advanced Oxidation Processes (AOPs) for Wastewater, Organic Pollutants and Pharmaceutical Waste Treatment: A Mini Review. *Chem. Eng.* **2022**, *6*, 8. [CrossRef]
2. Ushani, U.; Lu, X.; Wang, J.; Zhang, Z.; Dai, J.; Tan, Y.; Wang, S.; Li, W.; Niu, C.; Cai, T.; et al. Sulfate radicals-based advanced oxidation technology in various environmental remediation: A state-of-the–art review. *Chem. Eng. J.* **2020**, *402*, 126232. [CrossRef]
3. Brienza, M.; Katsoyiannis, I.A. Sulfate Radical Technologies as Tertiary Treatment for the Removal of Emerging Contaminants from Wastewater. *Sustainability* **2017**, *9*, 1604. [CrossRef]
4. Salazar, L.M.; Grisales, C.M.; Garcia, D.P. How does intensification influence the operational and environmental performance of photo-Fenton processes at acidic and circumneutral pH. *Environ. Sci. Pollut. Res.* **2018**, *26*, 4367–4380. [CrossRef] [PubMed]
5. Spasiano, D.; Marotta, R.; Malato, S.; Fernandez-Ibañez, P.; Di Somma, I. Solar photocatalysis: Materials, reactors, some commercial, and pre-industrialized applications. A comprehensive approach. *Appl. Catal. B Environ.* **2015**, *170–171*, 90–123. [CrossRef]
6. Dimian, A.C.; Bildea, C.S.; Kiss, A.A. Process Intensification. *Comput. Aided Chem. Eng.* **2014**, 397–448. [CrossRef]
7. Huang, K.; Wang, S.-J.; Shan, L.; Zhu, Q.; Qian, J. Seeking synergistic effect—A key principle in process intensification. *Sep. Purif. Technol.* **2007**, *57*, 111–120. [CrossRef]
8. Mesones, S.; Mena, E.; López-Muñoz, M.J.; Adán, C.; Marugán, J. Synergistic and antagonistic effects in the photoelectrocatalytic disinfection of water with TiO_2 supported on activated carbon as a bipolar electrode in a novel 3D photoelectrochemical reactor. *Sep. Purif. Technol.* **2020**, *247*, 117002. [CrossRef]
9. Malato, S.; Fernández-Ibáñez, P.; Maldonado, M.; Blanco, J.; Gernjak, W. Decontamination and disinfection of water by solar photocatalysis: Recent overview and trends. *Catal. Today* **2009**, *147*, 1–59. [CrossRef]
10. Herrmann, J.-M. Photocatalysis fundamentals revisited to avoid several misconceptions. *Appl. Catal. B Environ.* **2010**, *99*, 461–468. [CrossRef]
11. Azzaz, A.; Jellali, S.; Hamed, N.; El Jery, A.; Khezami, L.; Assadi, A.; Amrane, A. Photocatalytic Treatment of Wastewater Containing Simultaneous Organic and Inorganic Pollution: Competition and Operating Parameters Effects. *Catalysts* **2021**, *11*, 855. [CrossRef]
12. Ochoa-Gutiérrez, K.S.; Tabares-Aguilar, E.; Mueses, M.; Machuca-Martínez, F.; Puma, G.L. A Novel Prototype Offset Multi Tubular Photoreactor (OMTP) for solar photocatalytic degradation of water contaminants. *Chem. Eng. J.* **2018**, *341*, 628–638. [CrossRef]
13. Elhalil, A.; Elmoubarki, R.; Farnane, M.; Machrouhi, A.; Sadiq, M.; Mahjoubi, F.; Qourzal, S.; Barka, N. Photocatalytic degradation of caffeine as a model pharmaceutical pollutant on Mg doped ZnO-Al_2O_3 heterostructure. *Environ. Nanotechnol. Monit. Manag.* **2018**, *10*, 63–72. [CrossRef]
14. Jallouli, N.; Pastrana-Martínez, L.M.; Ribeiro, A.R.; Moreira, N.F.; Faria, J.L.; Hentati, O.; Silva, A.M.; Ksibi, M. Heterogeneous photocatalytic degradation of ibuprofen in ultrapure water, municipal and pharmaceutical industry wastewaters using a TiO_2/UV-LED system. *Chem. Eng. J.* **2018**, *334*, 976–984. [CrossRef]
15. León, D.E.; Zúñiga-Benítez, H.; Peñuela, G.A.; Mansilla, H.D. Photocatalytic Removal of the Antibiotic Cefotaxime on TiO_2 and ZnO Suspensions Under Simulated Sunlight Radiation. *Water Air Soil Pollut.* **2017**, *228*, 361. [CrossRef]
16. Martínez, C.; Fernández, M.I.; Santaballa, J.A.; Faria, J. Aqueous degradation of diclofenac by heterogeneous photocatalysis using nanostructured materials. *Appl. Catal. B Environ.* **2011**, *107*, 110–118. [CrossRef]
17. Garrido, I.; Flores, P.; Hellín, P.; Vela, N.; Navarro, S.; Fenoll, J. Solar reclamation of agro-wastewater polluted with eight pesticides by heterogeneous photocatalysis using a modular facility. A case study. *Chemosphere* **2020**, *249*, 126156. [CrossRef]
18. Wang, B.; Fu, T.; An, B.; Liu, Y. UV light-assisted persulfate activation by Cu^0-Cu_2O for the degradation of sulfamerazine. *Sep. Purif. Technol.* **2020**, *251*, 117321. [CrossRef]
19. Tao, Y.; Ni, Q.; Wei, M.; Xia, D.; Li, X.; Xu, A. Metal-free activation of peroxymonosulfate by g-C_3N_4 under visible light irradiation for the degradation of organic dyes. *RSC Adv.* **2015**, *5*, 44128–44136. [CrossRef]

20. Casado, C.; Marugán, J.; Timmers, R.; Muñoz, M.; van Grieken, R. Comprehensive multiphysics modeling of photocatalytic processes by computational fluid dynamics based on intrinsic kinetic parameters determined in a differential photoreactor. *Chem. Eng. J.* **2017**, *310*, 368–380. [CrossRef]
21. Carbajo, J.; Tolosana-Moranchel, A.; Casas, J.A.; Faraldos, M.; Bahamonde, A. Analysis of photoefficiency in TiO_2 aqueous suspensions: Effect of titania hydrodynamic particle size and catalyst loading on their optical properties. *Appl. Catal. B Environ.* **2018**, *221*, 1–8. [CrossRef]
22. Tolosana-Moranchel, A.; Casas, J.; Carbajo, J.; Faraldos, M.; Bahamonde, A. Influence of TiO_2 optical parameters in a slurry photocatalytic reactor: Kinetic modelling. *Appl. Catal. B Environ.* **2017**, *200*, 164–173. [CrossRef]
23. Acosta-Herazo, R.; Mueses, M.; Puma, G.L.; Machuca-Martínez, F. Impact of photocatalyst optical properties on the efficiency of solar photocatalytic reactors rationalized by the concepts of initial rate of photon absorption (IRPA) dimensionless boundary layer of photon absorption and apparent optical thickness. *Chem. Eng. J.* **2018**, *356*, 839–849. [CrossRef]
24. Grčić, I.; Puma, G.L. Six-flux absorption-scattering models for photocatalysis under wide-spectrum irradiation sources in annular and flat reactors using catalysts with different optical properties. *Appl. Catal. B Environ.* **2017**, *211*, 222–234. [CrossRef]
25. Koltsakidou, A.; Antonopoulou, M.; Sykiotou, M.; Evgenidou, E.; Konstantinou, I.; Lambropoulou, D. Photo-Fenton and Fenton-like processes for the treatment of the antineoplastic drug 5-fluorouracil under simulated solar radiation. *Environ. Sci. Pollut. Res.* **2016**, *24*, 4791–4800. [CrossRef] [PubMed]
26. Villota, N.; Ferreiro, C.; Qulatein, H.; Lomas, J.; Lombraña, J. Turbidity Changes during Carbamazepine Oxidation by Photo-Fenton. *Catalysts* **2021**, *11*, 894. [CrossRef]
27. Coelho, A.; Castro, A.V.; Dezotti, M.; Sant'Anna, G. Treatment of petroleum refinery sourwater by advanced oxidation processes. *J. Hazard. Mater.* **2006**, *137*, 178–184. [CrossRef] [PubMed]
28. Cabrera-Reina, A.; Miralles-Cuevas, S.; López, J.C.; Pérez, J.S. Pyrimethanil degradation by photo-Fenton process: Influence of iron and irradiance level on treatment cost. *Sci. Total Environ.* **2017**, *605-606*, 230–237. [CrossRef]
29. Ahmed, S.; Rasul, M.G.; Martens, W.N.; Brown, R.; Hashib, M.A. Heterogeneous photocatalytic degradation of phenols in wastewater: A review on current status and developments. *Desalination* **2010**, *261*, 3–18. [CrossRef]
30. Seid, M.G.; Byun, J.; Kim, W.; Cho, K.; Hong, S.W. Changes in levels of N-nitrosamine formed from amine-containing compounds during chloramination via photocatalytic pretreatment with immobilized TiO_2: Effect of source water and pH. *J. Hazard. Mater.* **2021**, *424*, 127398. [CrossRef]
31. Azeez, F.; Al-Hetlani, E.; Arafa, M.; Abdelmonem, Y.; Nazeer, A.A.; Amin, M.O.; Madkour, M. The effect of surface charge on photocatalytic degradation of methylene blue dye using chargeable titania nanoparticles. *Sci. Rep.* **2018**, *8*, 7104. [CrossRef] [PubMed]
32. Carbajo, J.; Jiménez, M.; Miralles, S.; Malato, S.; Faraldos, M.; Bahamonde, A. Study of application of titania catalysts on solar photocatalysis: Influence of type of pollutants and water matrices. *Chem. Eng. J.* **2016**, *291*, 64–73. [CrossRef]
33. Mirzaei, A.; Chen, Z.; Haghighat, F.; Yerushalmi, L. Removal of pharmaceuticals from water by homo/heterogonous Fenton-type processes—A review. *Chemosphere* **2017**, *174*, 665–688. [CrossRef]
34. Cavalcante, R.P.; Sandim, L.D.R.; Bogo, D.; Barbosa, A.M.J.; Osugi, M.E.; Blanco, M.; De Oliveira, S.C.; Matos, M.D.F.C.; Machulek, A.; Ferreira, V.S. Application of Fenton, photo-Fenton, solar photo-Fenton, and UV/H_2O_2 to degradation of the antineoplastic agent mitoxantrone and toxicological evaluation. *Environ. Sci. Pollut. Res.* **2012**, *20*, 2352–2361. [CrossRef] [PubMed]
35. Governo, M.; Santos, M.S.F.; Alves, A.; Madeira, L.M. Degradation of the cytostatic 5-Fluorouracil in water by Fenton and photo-assisted oxidation processes. *Environ. Sci. Pollut. Res.* **2016**, *24*, 844–854. [CrossRef]
36. Elmolla, E.S.; Chaudhuri, M. Degradation of the antibiotics amoxicillin, ampicillin and cloxacillin in aqueous solution by the photo-Fenton process. *J. Hazard. Mater.* **2009**, *172*, 1476–1481. [CrossRef]
37. El Shahawy, A.; Mohamadien, R.H.; El-Fawal, E.M.; Moustafa, Y.M.; Dawood, M.M.K. Hybrid Photo-Fenton oxidation and biosorption for petroleum wastewater treatment and optimization using Box–Behnken Design. *Environ. Technol. Innov.* **2021**, *24*, 101834. [CrossRef]
38. Tawfik, A.; Alalm, M.G.; Awad, H.M.; Islam, M.; Qyyum, M.A.; Al-Muhtaseb, A.H.; Osman, A.I.; Lee, M. Solar photo-oxidation of recalcitrant industrial wastewater: A review. *Environ. Chem. Lett.* **2022**, *20*, 1839–1862. [CrossRef]
39. Arzate, S.; Campos-Mañas, M.; Miralles-Cuevas, S.; Agüera, A.; Sánchez, J.G.; Pérez, J.S. Removal of contaminants of emerging concern by continuous flow solar photo-Fenton process at neutral pH in open reactors. *J. Environ. Manag.* **2020**, *261*, 110265. [CrossRef] [PubMed]
40. Prada-Vásquez, M.A.; Estrada-Flórez, S.E.; Serna-Galvis, E.A.; Torres-Palma, R.A. Developments in the intensification of photo-Fenton and ozonation-based processes for the removal of contaminants of emerging concern in Ibero-American countries. *Sci. Total Environ.* **2020**, *765*, 142699. [CrossRef]
41. Clarizia, L.; Russo, D.; Di Somma, I.; Marotta, R.; Andreozzi, R. Homogeneous photo-Fenton processes at near neutral pH: A review. *Appl. Catal. B Environ.* **2017**, *209*, 358–371. [CrossRef]
42. Silva, G.D.; Marson, E.O.; Batista, L.L.; Ueira-Vieira, C.; Starling, M.C.V.; Trovó, A.G. Contrasting the performance of photo-Fenton at neutral pH in the presence of different organic iron-complexes using hydrogen peroxide or persulfate as oxidants for naproxen degradation and removal of antimicrobial activity. *Process. Saf. Environ. Prot.* **2021**, *147*, 798–807. [CrossRef]
43. Cai, C.; Zhang, Z.; Liu, J.; Shan, N.; Zhang, H.; Dionysiou, D.D. Visible light-assisted heterogeneous Fenton with $ZnFe_2O_4$ for the degradation of Orange II in water. *Appl. Catal. B Environ.* **2016**, *182*, 456–468. [CrossRef]

44. Ma, J.; Yang, Q.; Wen, Y.; Liu, W. Fe-g-C_3N_4/graphitized mesoporous carbon composite as an effective Fenton-like catalyst in a wide pH range. *Appl. Catal. B Environ.* **2017**, *201*, 232–240. [CrossRef]
45. Arzate-Salgado, S.-Y.; Morales-Pérez, A.-A.; Solís-López, M.; Ramírez-Zamora, R.-M. Evaluation of metallurgical slag as a Fenton-type photocatalyst for the degradation of an emerging pollutant: Diclofenac. *Catal. Today* **2016**, *266*, 126–135. [CrossRef]
46. Buitrago, J.L.; Sanabria, J.; Gútierrez-Zapata, H.M.; Urbano-Ceron, F.J.; García-Barco, A.; Osorio-Vargas, P.; Rengifo-Herrera, J.A. Photo-Fenton process at natural conditions of pH, iron, ions, and humic acids for degradation of diuron and amoxicillin. *Environ. Sci. Pollut. Res.* **2019**, *27*, 1608–1624. [CrossRef]
47. De la Cruz, N.; Esquius, L.; Grandjean, D.; Magnet, A.; Tungler, A.; de Alencastro, L.; Pulgarín, C. Degradation of emergent contaminants by UV, UV/H_2O_2 and neutral photo-Fenton at pilot scale in a domestic wastewater treatment plant. *Water Res.* **2013**, *47*, 5836–5845. [CrossRef] [PubMed]
48. Tambat, S.; Umale, S.; Sontakke, S. Photocatalytic degradation of Milling Yellow dye using sol–gel synthesized CeO. *Mater. Res. Bull.* **2016**, *76*, 466–472. [CrossRef]
49. Lin, Y.-C.; Lee, H.-S. Effects of TiO_2 coating dosage and operational parameters on a TiO_2/Ag photocatalysis system for decolorizing Procion red MX-5B. *J. Hazard. Mater.* **2010**, *179*, 462–470. [CrossRef]
50. Chen, Y.-W.; Hsu, Y.-H. Effects of Reaction Temperature on the Photocatalytic Activity of TiO_2 with Pd and Cu Cocatalysts. *Catalysts* **2021**, *11*, 966. [CrossRef]
51. Silveira, J.E.; Garcia-Costa, A.L.; Carbajo, J.; Ribeiro, A.R.; Pliego, G.; Paz, W.S.; Zazo, J.A.; Casas, J.A. Nitrate removal in saline water by photo-reduction using natural $FeTiO_3$ as catalyst. *Chem. Eng. J. Adv.* **2022**, *12*, 100387. [CrossRef]
52. Bloh, J.Z. Intensification of Heterogeneous Photocatalytic Reactions Without Efficiency Losses: The Importance of Surface Catalysis. *Catal. Lett.* **2021**, *151*, 3105–3113. [CrossRef]
53. Prieto-Rodríguez, L.; Spasiano, D.; Oller, I.; Fernández-Calderero, I.; Agüera, A.; Malato, S. Solar photo-Fenton optimization for the treatment of MWTP effluents containing emerging contaminants. *Catal. Today* **2013**, *209*, 188–194. [CrossRef]
54. Pérez, M.; Torrades, F.; Domènech, X.; Peral, J. Fenton and photo-Fenton oxidation of textile effluents. *Water Res.* **2001**, *36*, 2703–2710. [CrossRef]
55. Torrades, F.; Pérez, M.; Mansilla, H.D.; Peral, J. Experimental design of Fenton and photo-Fenton reactions for the treatment of cellulose bleaching effluents. *Chemosphere* **2003**, *53*, 1211–1220. [CrossRef] [PubMed]
56. Sagawe, G.; Lehnard, A.; Lübber, M.; Bahnemann, D. The insulated solar fenton hybrid process: Fundamental investi-gations. *Helv. Chim. Acta* **2001**, *84*, 3742–3759. [CrossRef]
57. Gernjak, W.; Fuerhacker, M.; Fernández-Ibañez, P.; Blanco, J.; Malato, S. Solar photo-Fenton treatment—Process parameters and process control. *Appl. Catal. B Environ.* **2006**, *64*, 121–130. [CrossRef]
58. Zhang, J.; Zhang, X.; Wang, Y. Degradation of phenol by a heterogeneous photo-Fenton process using Fe/Cu/Al catalysts. *RSC Adv.* **2016**, *6*, 13168–13176. [CrossRef]
59. Expósito, A.J.; Monteagudo, J.M.; Díaz, I.; Durán, A. Photo-fenton degradation of a beverage industrial effluent: Intensification with persulfate and the study of radicals. *Chem. Eng. J.* **2016**, *306*, 1203–1211. [CrossRef]
60. Zapata, A.; Oller, I.; Bizani, E.; Sánchez-Pérez, J.; Maldonado, M.; Malato, S. Evaluation of operational parameters involved in solar photo-Fenton degradation of a commercial pesticide mixture. *Catal. Today* **2009**, *144*, 94–99. [CrossRef]
61. Carbajo, J.; Silveira, J.; Pliego, G.; Zazo, J.; Casas, J. Increasing Photo-Fenton process Efficiency: The effect of high temperatures. *Sep. Purif. Technol.* **2021**, *271*, 118876. [CrossRef]
62. Vallés, I.; Santos-Juanes, L.; Amat, A.; Moreno-Andrés, J.; Arques, A. Effect of Salinity on UVA-Vis Light Driven Photo-Fenton Process at Acidic and Circumneutral pH. *Water* **2021**, *13*, 1315. [CrossRef]
63. Pliego, G.; Xekoukoulotakis, N.; Venieri, D.; Zazo, J.A.; Casas, J.A.; Rodriguez, J.J.; Mantzavinos, D. Complete degradation of the persistent anti-depressant sertraline in aqueous solution by solar photo-Fenton oxidation. *J. Chem. Technol. Biotechnol.* **2014**, *89*, 814–818. [CrossRef]
64. Hermosilla, D.; Merayo, N.; Ordóñez, R.; Blanco, Á. Optimization of conventional Fenton and ultraviolet-assisted oxidation processes for the treatment of reverse osmosis retentate from a paper mill. *Waste Manag.* **2012**, *32*, 1236–1243. [CrossRef]
65. Pouran, S.R.; Aziz, A.A.; Daud, W.M.A.W. Review on the main advances in photo-Fenton oxidation system for recalcitrant wastewaters. *J. Ind. Eng. Chem.* **2015**, *21*, 53–69. [CrossRef]
66. Sirtori, C.; Zapata, A.; Gernjak, W.; Malato, S.; Lopez, A.; Agüera, A. Solar photo-Fenton degradation of nalidixic acid in waters and wastewaters of different composition. Analytical assessment by LC–TOF-MS. *Water Res.* **2011**, *45*, 1736–1744. [CrossRef]
67. Hermosilla, D.; Cortijo, M.; Huang, C.P. Optimizing the treatment of landfill leachate by conventional Fenton and photo-Fenton processes. *Sci. Total Environ.* **2009**, *407*, 3473–3481. [CrossRef]
68. Cunha-Filho, F.J.; Mota-Lima, A.; Ratkievicius, L.A.; Silva, D.J.; Silva, D.N.; Chiavone-Filho, O.; Nascimento, C.A.O.D. Rapid mineralization rate of acetylsalicylic acid in a tubular photochemical reactor: The role of the optimized excess of H_2O_2. *J. Water Process. Eng.* **2019**, *31*, 100856. [CrossRef]
69. Batista, A.P.S.; Nogueira, R.F.P. Parameters affecting sulfonamide photo-Fenton degradation–Iron complexation and substituent group. *J. Photochem. Photobiol. A Chem.* **2012**, *232*, 8–13. [CrossRef]
70. Chu, W.; Chan, K.; Kwan, C.; Choi, K. Degradation of atrazine by modified stepwise-Fenton's processes. *Chemosphere* **2007**, *67*, 755–761. [CrossRef]

71. Monteagudo, J.; Durán, A.; Martín, I.S.; Aguirre, M. Effect of continuous addition of H_2O_2 and air injection on ferrioxalate-assisted solar photo-Fenton degradation of Orange II. *Appl. Catal. B Environ.* **2009**, *89*, 510–518. [CrossRef]
72. Prieto-Rodríguez, L.; Oller, I.; Zapata, A.; Agüera, A.; Malato, S. Hydrogen peroxide automatic dosing based on dissolved oxygen concentration during solar photo-Fenton. *Catal. Today* **2011**, *161*, 247–254. [CrossRef]
73. Yu, X.; Somoza-Tornos, A.; Graells, M.; Pérez-Moya, M. An experimental approach to the optimization of the dosage of hydrogen peroxide for Fenton and photo-Fenton processes. *Sci. Total Environ.* **2020**, *743*, 140402. [CrossRef] [PubMed]
74. Saldaña-Flores, K.E.; Flores-Estrella, R.A.; Alcaraz-Gonzalez, V.; Carissimi, E.; de Souza, B.G.; Ruotolo, L.A.M.; Urquieta-Gonzalez, E. Regulation of Hydrogen Peroxide Dosage in a Heterogeneous Photo-Fenton Process. *Processes* **2021**, *9*, 2167. [CrossRef]
75. Silva, T.F.; Fonseca, A.; Saraiva, I.; Boaventura, R.A.; Vilar, V.J. Scale-up and cost analysis of a photo-Fenton system for sanitary landfill leachate treatment. *Chem. Eng. J.* **2015**, *283*, 76–88. [CrossRef]
76. Devi, L.G.; Srinivas, M.; ArunaKumari, M. Heterogeneous advanced photo- Fenton process using peroxymonosulfate and peroxydisulfate in presence of zero valent metallic iron: A comparative study with hydrogen peroxide photo-Fenton process. *J. Water Process. Eng.* **2016**, *13*, 117–126. [CrossRef]
77. Giannakis, S.; Lin, K.-Y.A.; Ghanbari, F. A review of the recent advances on the treatment of industrial wastewaters by Sulfate Radical-based Advanced Oxidation Processes (SR-AOPs). *Chem. Eng. J.* **2020**, *406*, 127083. [CrossRef]
78. Ge, M.; Hu, Z.; Wei, J.; He, Q.; He, Z. Recent advances in persulfate-assisted TiO_2-based photocatalysis for wastewater treatment: Performances, mechanism and perspectives. *J. Alloys Compd.* **2021**, *888*, 161625. [CrossRef]
79. Ismail, L.; Ferronato, C.; Fine, L.; Jaber, F.; Chovelon, J.-M. Elimination of sulfaclozine from water with SO_4-radicals: Evaluation of different persulfate activation methods. *Appl. Catal. B Environ.* **2017**, *201*, 573–581. [CrossRef]
80. Ding, H.; Hu, J. Degradation of ibuprofen by UVA-LED/TiO_2/persulfate process: Kinetics, mechanism, water matrix effects, intermediates and energy consumption. *Chem. Eng. J.* **2020**, *397*, 125462. [CrossRef]
81. Du, X.; Bai, X.; Xu, L.; Yang, L.; Jin, P. Visible-light activation of persulfate by TiO_2/g-C_3N_4 photocatalyst toward efficient degradation of micropollutants. *Chem. Eng. J.* **2019**, *384*, 123245. [CrossRef]
82. Carbajo, J.; Adán, C.; Rey, A.; Martínez-Arias, A.; Bahamonde, A. Optimization of H_2O_2 use during the photocatalytic degradation of ethidium bromide with TiO_2 and iron-doped TiO_2 catalysts. *Appl. Catal. B Environ.* **2010**, *102*, 85–93. [CrossRef]
83. Cuervo Lumbaque, E.; Sirtori, C.; Vilar, V.J. Heterogeneous photocatalytic degradation of pharmaceuticals in synthetic and real matrices using a tube-in-tube membrane reactor with radial addition of H_2O_2. *Sci. Total Environ.* **2020**, *743*, 140629. [CrossRef]
84. Fu, Y.; Chang, C.; Chen, P.; Chu, X.; Zhu, L. Enhanced photocatalytic performance of boron doped Bi2WO6 nanosheets under simulated solar light irradiation. *J. Hazard. Mater.* **2013**, *254*, 185–192. [CrossRef]
85. García-Muñoz, P.; Zussblatt, N.P.; Pliego, G.; Zazo, J.A.; Fresno, F.; Chmelka, B.F.; Casas, J.A. Evaluation of photoassisted treatments for norfloxacin removal in water using mesoporous Fe_2O_3-TiO_2 materials. *J. Environ. Manag.* **2019**, *238*, 243–250. [CrossRef]
86. Ismail, A.A.; Abdelfattah, I.; Faisal, M.; Helal, A. Efficient photodecomposition of herbicide imazapyr over mesoporous Ga_2O_3-TiO_2 nanocomposites. *J. Hazard. Mater.* **2018**, *342*, 519–526. [CrossRef]
87. Phan, T.T.N.; Nikoloski, A.N.; Bahri, P.A.; Li, D. Adsorption and photo-Fenton catalytic degradation of organic dyes over crystalline $LaFeO_3$-doped porous silica. *RSC Adv.* **2018**, *8*, 36181–36190. [CrossRef]
88. Phan, T.T.N.; Nikoloski, A.N.; Bahri, P.A.; Li, D. Enhanced removal of organic using $LaFeO_3$-integrated modified natural zeolites via heterogeneous visible light photo-Fenton degradation. *J. Environ. Manag.* **2018**, *233*, 471–480. [CrossRef]
89. Wang, G.; Wang, X.; Liu, J.; Sun, X. Mesoporous Au/TiO_2 Nanocomposite Microspheres for Visible-Light Photocatalysis. *Chem. Eur. J.* **2012**, *18*, 5361–5366. [CrossRef]
90. Wu, Y.; Qin, L.; Zhang, G.; Chen, L.; Guo, X.; Liu, M. Porous Solid Superacid SO_4^{2-}/$Fe_{2-x}Zr_xO_3$ Fenton Catalyst for Highly Effective Oxidation of X-3B under Visible Light. *Ind. Eng. Chem. Res.* **2013**, *52*, 16698–16708. [CrossRef]
91. Simsek, E.B.; Tuna, Ö.; Balta, Z. Construction of stable perovskite-type $LaFeO_3$ particles on polymeric resin with boosted photocatalytic Fenton-like decaffeination under solar irradiation. *Sep. Purif. Technol.* **2019**, *237*, 116384. [CrossRef]
92. Barik, A.J.; Gogate, P.R. Degradation of 4-chloro 2-aminophenol using combined strategies based on ultrasound, photolysis and ozone. *Ultrason. Sonochem.* **2016**, *28*, 90–99. [CrossRef]
93. Sheydaei, M.; Zangouei, M.; Vatanpour, V. Coupling visible light sono-photocatalysis and sono-enhanced ultrafiltration processes for continuous flow degradation of dyestuff using N-doped titania nanoparticles. *Chem. Eng. Process. Process. Intensif.* **2019**, *143*. [CrossRef]
94. Kakavandi, B.; Bahari, N.; Kalantary, R.R.; Fard, E.D. Enhanced sono-photocatalysis of tetracycline antibiotic using TiO_2 decorated on magnetic activated carbon (MAC@T) coupled with US and UV: A new hybrid system. *Ultrason. Sonochem.* **2019**, *55*, 75–85. [CrossRef]
95. Babu, S.G.; Karthik, P.; John, M.C.; Lakhera, S.K.; Ashokkumar, M.; Khim, J.; Neppolian, B. Synergistic effect of sono-photocatalytic process for the degradation of organic pollutants using CuO-TiO_2/rGO. *Ultrason. Sonochem.* **2018**, *50*, 218–223. [CrossRef]
96. Geng, N.; Chen, W.; Xu, H.; Lin, T.; Ding, M.; Wang, Y.; Tao, H.; Hu, K. Preparation of Fe_3O_4/TiO_2-N-GO sonocatalyst and using for humic acid removal with the assist of ultrasound. *Mater. Sci. Semicond. Process.* **2019**, *102*, 104593. [CrossRef]
97. Isari, A.A.; Hayati, F.; Kakavandi, B.; Rostami, M.; Motevassel, M.; Dehghanifard, E. N, Cu co-doped TiO_2@functionalized SWCNT photocatalyst coupled with ultrasound and visible-light: An effective sono-photocatalysis process for pharmaceutical wastewaters treatment. *Chem. Eng. J.* **2019**, *392*, 123685. [CrossRef]

98. Eshaq, G.; Wang, S.; Sun, H.; Sillanpää, M. Core/shell $FeVO_4$@BiOCl heterojunction as a durable heterogeneous Fenton catalyst for the efficient sonophotocatalytic degradation of p-nitrophenol. *Sep. Purif. Technol.* **2019**, *231*, 115915. [CrossRef]
99. Guan, S.; Yang, H.; Sun, X.; Xian, T. Preparation and promising application of novel $LaFeO_3$/BiOBr heterojunction photocatalysts for photocatalytic and photo-Fenton removal of dyes. *Opt. Mater.* **2019**, *100*, 109644. [CrossRef]
100. Hu, J.; Li, J.; Cui, J.; An, W.; Liu, L.; Liang, Y.; Cui, W. Surface oxygen vacancies enriched FeOOH/Bi_2MoO_6 photocatalysis- fenton synergy degradation of organic pollutants. *J. Hazard. Mater.* **2019**, *384*, 121399. [CrossRef]
101. Huang, S.; Zhang, Q.; Liu, P.; Ma, S.; Xie, B.; Yang, K.; Zhao, Y. Novel up-conversion carbon quantum dots/α-FeOOH nanohybrids eliminate tetracycline and its related drug resistance in visible-light responsive Fenton system. *Appl. Catal. B Environ.* **2019**, *263*, 118336. [CrossRef]
102. Li, Q.; Kong, H.; Li, P.; Shao, J.; He, Y. Photo-Fenton degradation of amoxicillin via magnetic TiO_2-graphene oxide-Fe_3O_4 composite with a submerged magnetic separation membrane photocatalytic reactor (SMSMPR). *J. Hazard. Mater.* **2019**, *373*, 437–446. [CrossRef]
103. Manickam-Periyaraman, P.; Espinosa, J.C.; Ferrer, B.; Subramanian, S.; Álvaro, M.; García, H.; Navalón, S. Bimetallic iron-copper oxide nanoparticles supported on nanometric diamond as efficient and stable sunlight-assisted Fenton photocatalyst. *Chem. Eng. J.* **2020**, *393*, 124770. [CrossRef]
104. García-Muñoz, P.; Pliego, G.; Zazo, J.; Bahamonde, A.; Casas, J. Ilmenite ($FeTiO_3$) as low cost catalyst for advanced oxidation processes. *J. Environ. Chem. Eng.* **2016**, *4*, 542–548. [CrossRef]
105. Arshad, A.; Iqbal, J.; Ahmad, I.; Israr, M. Graphene/Fe_3O_4 nanocomposite: Interplay between photo-Fenton type reaction, and carbon purity for the removal of methyl orange. *Ceram. Int.* **2018**, *44*, 2643–2648. [CrossRef]
106. Desipio, M.M.; Van Bramer, S.E.; Thorpe, R.; Saha, D. Photocatalytic and photo-fenton activity of iron oxide-doped carbon nitride in 3D printed and LED driven photon concentrator. *J. Hazard. Mater.* **2019**, *376*, 178–187. [CrossRef]
107. Garcia-Muñoz, P.; Lefevre, C.; Robert, D.; Keller, N. Ti-substituted $LaFeO_3$ perovskite as photoassisted CWPO catalyst for water treatment. *Appl. Catal. B Environ.* **2019**, *248*, 120–128. [CrossRef]
108. Garcia-Muñoz, P.; Fresno, F.; Lefevre, C.; Robert, D.; Keller, N. Highly robust $La_{1-x}Ti_xFeO_3$ dual catalyst with combined photocatalytic and photo-CWPO activity under visible light for 4-chlorophenol removal in water. *Appl. Catal. B Environ.* **2019**, *262*, 118310. [CrossRef]
109. Wang, Q.; Wang, P.; Xu, P.; Li, Y.; Duan, J.; Zhang, G.; Hu, L.; Wang, X.; Zhang, W. Visible-light-driven photo-Fenton reactions using $Zn_{1\text{-}1.5}Fe$ S/g-C_3N_4 photocatalyst: Degradation kinetics and mechanisms analysis. *Appl. Catal. B Environ.* **2020**, *266*, 118653. [CrossRef]
110. Yang, L.; Jiao, Y.; Xu, X.; Pan, Y.; Su, C.; Duan, X.; Sun, H.; Liu, S.; Wang, S.; Shao, Z. Superstructures with Atomic-Level Arranged Perovskite and Oxide Layers for Advanced Oxidation with an Enhanced Non-Free Radical Pathway. *ACS Sustain. Chem. Eng.* **2022**, *10*, 1899–1909. [CrossRef]
111. García-Muñoz, P.; Pliego, G.; Zazo, J.A.; Casas, J.A. Photocatalytic wet peroxide oxidation process at circumneutral pH using ilmenite as catalyst. *J. Environ. Chem. Eng.* **2018**, *6*, 7312–7317. [CrossRef]
112. García-Muñoz, P.; Pliego, G.; Zazo, J.; Bahamonde, A.; Casas, J. Sulfonamides photoassisted oxidation treatments catalyzed by ilmenite. *Chemosphere* **2017**, *180*, 523–530. [CrossRef] [PubMed]
113. García-Muñoz, P.; Pliego, G.; Zazo, J.; Barbero, B.; Bahamonde, A.; Casas, J. Modified ilmenite as catalyst for CWPO-Photoassisted process under LED light. *Chem. Eng. J.* **2017**, *318*, 89–94. [CrossRef]
114. Garcia-Muñoz, P.; Fresno, F.; Lefevre, C.; Robert, D.; Keller, N. Synergy effect between photocatalysis and heterogeneous photo-Fenton catalysis on Ti-doped $LaFeO_3$ perovskite for high efficiency light-assisted water treatment. *Catal. Sci. Technol.* **2020**, *10*, 1299–1310. [CrossRef]
115. Grilla, E.; Matthaiou, V.; Frontistis, Z.; Oller, I.; Polo, I.; Malato, S.; Mantzavinos, D. Degradation of antibiotic trimethoprim by the combined action of sunlight, TiO_2 and persulfate: A pilot plant study. *Catal. Today* **2018**, *328*, 216–222. [CrossRef]
116. Yentür, G.; Dükkancı, M. Fabrication of magnetically separable plasmonic composite photocatalyst of Ag/AgBr/$ZnFe_2O_4$ for visible light photocatalytic oxidation of carbamazepine. *Appl. Surf. Sci.* **2020**, *510*, 145374. [CrossRef]
117. Zhong, X.; Zou, Z.-S.; Wang, H.-L.; Huang, W.; Zhou, B.-X. Enhanced Activation of Persulfate by Co-Doped Bismuth Ferrite Nanocomposites for Degradation of Levofloxacin Under Visible Light Irradiation. *Materials* **2019**, *12*, 3952. [CrossRef]
118. Silveira, J.E.; Paz, W.S.; Garcia-Muñoz, P.; Zazo, J.A.; Casas, J.A. UV-LED/ilmenite/persulfate for azo dye mineralization: The role of sulfate in the catalyst deactivation. *Appl. Catal. B Environ.* **2017**, *219*, 314–321. [CrossRef]
119. Robert, D.; Keller, V.; Keller, N. Immobilization of a Semiconductor Photocatalyst on Solid Supports: Methods, Materials, and Applications. In *Photocatalysis and Water Purification: From Fundamentals to Recent Applications*; Wiley-VCH Verlag GmbH & Co. KGaA: Weinheim, Germany, 2013; pp. 145–178. [CrossRef]
120. Allé, P.H.; García-Muñoz, P.; Adouby, K.; Keller, N.; Robert, D. Efficient photocatalytic mineralization of polymethylmethacrylate and polystyrene nanoplastics by TiO_2/β-SiC alveolar foams. *Environ. Chem. Lett.* **2020**, *19*, 1803–1808. [CrossRef]
121. M'Bra, I.C.; García-Muñoz, P.; Drogui, P.; Keller, N.; Trokourey, A.; Robert, D. Heterogeneous photodegradation of Pyrimethanil and its commercial formulation with TiO_2 immobilized on SiC foams. *J. Photochem. Photobiol. A Chem.* **2019**, *368*, 1–6. [CrossRef]
122. Rico-Santacruz, M.; García-Muñoz, P.; Marchal, C.; Batail, N.; Pham, C.; Robert, D.; Keller, N. Coating-free TiO_2@β-SiC alveolar foams as a ready-to-use composite photocatalyst with tunable adsorption properties for water treatment. *RSC Adv.* **2020**, *10*, 3817–3825. [CrossRef] [PubMed]

123. Rico-Santacruz, M.; García-Muñoz, P.; Keller, V.; Batail, N.; Pham, C.; Robert, D.; Keller, N. Alveolar TiO_2-β-SiC photocatalytic composite foams with tunable properties for water treatment. *Catal. Today* **2018**, *328*, 235–242. [CrossRef]
124. Abdi, P.; Farzi, A.; Karimi, A. Application of a hybrid enzymatic and photo-fenton process for investigation of azo dye decolorization on TiO_2/metal-foam catalyst. *J. Taiwan Inst. Chem. Eng.* **2017**, *71*, 137–144. [CrossRef]
125. Orak, C.; Atalay, S.; Ersöz, G. Photocatalytic and photo-Fenton-like degradation of methylparaben on monolith-supported perovskite-type catalysts. *Sep. Sci. Technol.* **2017**, *52*, 1310–1320. [CrossRef]
126. Martín-Sómer, M.; Pablos, C.; de Diego, A.; van Grieken, R.; Encinas, A.; Monsalvo, V.M.; Marugán, J. Novel macroporous 3D photocatalytic foams for simultaneous wastewater disinfection and removal of contaminants of emerging concern. *Chem. Eng. J.* **2019**, *366*, 449–459. [CrossRef]
127. Dewil, R.; Mantzavinos, D.; Poulios, I.; Rodrigo, M.A. New perspectives for Advanced Oxidation Processes. *J. Environ. Manag.* **2017**, *195*, 93–99. [CrossRef]
128. Spuhler, D.; Rengifo-Herrera, J.A.; Pulgarin, C. The effect of Fe^{2+}, Fe^{3+}, H_2O_2 and the photo-Fenton reagent at near neutral pH on the solar disinfection (SODIS) at low temperatures of water containing *Escherichia coli* K12. *Appl. Catal. B Environ.* **2010**, *96*, 126–141. [CrossRef]
129. Pérez-Lucas, G.; Aliste, M.; Vela, N.; Garrido, I.; Fenoll, J.; Navarro, S. Decline of fluroxypyr and triclopyr residues from pure, drinking and leaching water by photo-assisted peroxonation. *Process. Saf. Environ. Prot.* **2020**, *137*, 358–365. [CrossRef]
130. Martini, J.; Orge, C.A.; Faria, J.L.; Pereira, M.F.R.; Soares, O.S.G. Sulfamethoxazole degradation by combination of advanced oxidation processes. *J. Environ. Chem. Eng.* **2018**, *6*, 4054–4060. [CrossRef]
131. Gmurek, M.; Gomes, J.F.; Martins, R.C.; Quinta-Ferreira, R.M. Comparison of radical-driven technologies applied for paraben mixture degradation: Mechanism, biodegradability, toxicity and cost assessment. *Environ. Sci. Pollut. Res.* **2019**, *26*, 37174–37192. [CrossRef]
132. Quiñones, D.H.; Álvarez, P.M.; Rey, A.; Contreras, S.; Beltrán, F.J. Application of solar photocatalytic ozonation for the degradation of emerging contaminants in water in a pilot plant. *Chem. Eng. J.* **2015**, *260*, 399–410. [CrossRef]
133. Roccamante, M.; Salmerón, I.; Ruiz, A.; Oller, I.; Malato, S. New approaches to solar Advanced Oxidation Processes for elimination of priority substances based on electrooxidation and ozonation at pilot plant scale. *Catal. Today* **2019**, *355*, 844–850. [CrossRef]
134. Rodríguez, E.M.; Rey, A.; Mena, E.; Beltrán, F.J. Application of solar photocatalytic ozonation in water treatment using supported TiO_2. *Appl. Catal. B Environ.* **2019**, *254*, 237–245. [CrossRef]
135. Buyukada, M. Removal, potential reaction pathways, and overall cost analysis of various pollution parameters and toxic odor compounds from the effluents of turkey processing plant using TiO_2–assisted UV/O_3 process. *J. Environ. Manag.* **2019**, *248*, 109298. [CrossRef] [PubMed]
136. Fathinia, M.; Khataee, A.; Naseri, A.; Aber, S. Monitoring simultaneous photocatalytic-ozonation of mixture of pharmaceuticals in the presence of immobilized TiO_2 nanoparticles using MCR-ALS: Identification of intermediates and multi-response optimization approach. *Spectrochim. Acta Part A Mol. Biomol. Spectrosc.* **2015**, *136*, 1275–1290. [CrossRef] [PubMed]
137. Fernandes, A.; Gągol, M.; Makoś, P.; Khan, J.A.; Boczkaj, G. Integrated photocatalytic advanced oxidation system (TiO_2/UV/O_3/H_2O_2) for degradation of volatile organic compounds. *Sep. Purif. Technol.* **2019**, *224*, 1–14. [CrossRef]
138. Rodríguez-Chueca, J.; Alonso, E.; Singh, D.N. Photocatalytic Mechanisms for Peroxymonosulfate Activation through the Removal of Methylene Blue: A Case Study. *Int. J. Environ. Res. Public Health* **2019**, *16*, 198. [CrossRef]
139. Talwar, S.; Verma, A.K.; Sangal, V.K.; Štangar, U.L. Once through continuous flow removal of metronidazole by dual effect of photo-Fenton and photocatalysis in a compound parabolic concentrator at pilot plant scale. *Chem. Eng. J.* **2020**, *388*, 124184. [CrossRef]
140. Salmerón, I.; Plakas, K.V.; Sirés, I.; Oller, I.; Maldonado, M.I.; Karabelas, A.J.; Malato, S. Optimization of electrocatalytic H_2O_2 production at pilot plant scale for solar-assisted water treatment. *Appl. Catal. B Environ.* **2018**, *242*, 327–336. [CrossRef]
141. Saleh, R.; Taufik, A. Degradation of methylene blue and congo-red dyes using Fenton, photo-Fenton, sono-Fenton, and sonophoto-Fenton methods in the presence of iron(II,III) oxide/zinc oxide/graphene (Fe_3O_4/ZnO/graphene) composites. *Sep. Purif. Technol.* **2018**, *210*, 563–573. [CrossRef]
142. Xu, L.; Chu, W.; Graham, N. Degradation of di-n-butyl phthalate by a homogeneous sono–photo–Fenton process with in situ generated hydrogen peroxide. *Chem. Eng. J.* **2014**, *240*, 541–547. [CrossRef]
143. Kouvelis, K.; Kampioti, A.A.; Petala, A.; Frontistis, Z. Degradation of Sulfamethoxazole Using a Hybrid CuO_x–$BiVO_4$/SPS/Solar System. *Catalysts* **2022**, *12*, 882. [CrossRef]
144. Liu, C.; Mao, S.; Shi, M.; Wang, F.; Xia, M.; Chen, Q.; Ju, X. Peroxymonosulfate activation through 2D/2D Z-scheme CoAl-LDH//BiOBr photocatalyst under visible light for ciprofloxacin degradation. *J. Hazard. Mater.* **2021**, *420*, 126613. [CrossRef]
145. Liu, C.; Mao, S.; Wang, H.; Wu, Y.; Wang, F.; Xia, M.; Chen, Q. Peroxymonosulfate-assisted for facilitating photocatalytic degradation performance of 2D/2D WO3/BiOBr S-scheme heterojunction. *Chem. Eng. J.* **2021**, *430*, 132806. [CrossRef]
146. Marjanovic, M.; Giannakis, S.; Grandjean, D.; de Alencastro, L.F.; Pulgarin, C. Effect of μM Fe addition, mild heat and solar UV on sulfate radical-mediated inactivation of bacteria, viruses, and micropollutant degradation in water. *Water Res.* **2018**, *140*, 220–231. [CrossRef]
147. Rodríguez-Chueca, J.; Giannakis, S.; Marjanovic, M.; Kohantorabi, M.; Gholami, M.R.; Grandjean, D.; de Alencastro, L.F.; Pulgarín, C. Solar-assisted bacterial disinfection and removal of contaminants of emerging concern by Fe^{2+}-activated HSO5-vs. $S_2O_8^{2-}$ in drinking water. *Appl. Catal. B Environ.* **2019**, *248*, 62–72. [CrossRef]

148. Rodríguez-Chueca, J.; Mesones, S.; Marugán, J. Hybrid UV-C/microfiltration process in membrane photoreactor for wastewater disinfection. *Environ. Sci. Pollut. Res.* **2018**, *26*, 36080–36087. [CrossRef] [PubMed]
149. Aydiner, C.; Mert, B.K.; Dogan, E.C.; Yatmaz, H.C.; Dagli, S.; Aksu, S.; Tilki, Y.M.; Goren, A.Y.; Balci, E. Novel hybrid treatments of textile wastewater by membrane oxidation reactor: Performance investigations, optimizations and efficiency comparisons. *Sci. Total Environ.* **2019**, *683*, 411–426. [CrossRef] [PubMed]
150. Moslehyani, A.; Mobaraki, M.; Matsuura, T.; Ismail, A.; Othman, M.; Chowdhury, M. Novel green hybrid processes for oily water photooxidation and purification from merchant ship. *Desalination* **2016**, *391*, 98–104. [CrossRef]
151. Kakavandi, B.; Ahmadi, M. Efficient treatment of saline recalcitrant petrochemical wastewater using heterogeneous UV-assisted sono-Fenton process. *Ultrason. Sonochem.* **2019**, *56*, 25–36. [CrossRef]
152. Raut-Jadhav, S.; Saharan, V.K.; Pinjari, D.V.; Saini, D.R.; Sonawane, S.H.; Pandit, A.B. Intensification of degradation of imidacloprid in aqueous solutions by combination of hydrodynamic cavitation with various advanced oxidation processes (AOPs). *J. Environ. Chem. Eng.* **2013**, *1*, 850–857. [CrossRef]
153. Sun, B.; Wang, Y.; Xiang, Y.; Shang, C. Influence of pre-ozonation of DOM on micropollutant abatement by UV-based advanced oxidation processes. *J. Hazard. Mater.* **2020**, *391*, 122201. [CrossRef] [PubMed]
154. Ghanbari, F.; Wu, J.; Khatebasreh, M.; Ding, D.; Lin, K.-Y.A. Efficient treatment for landfill leachate through sequential electrocoagulation, electrooxidation and PMS/UV/$CuFe_2O_4$ process. *Sep. Purif. Technol.* **2020**, *242*, 116828. [CrossRef]
155. Webler, A.D.; Moreira, F.C.; Dezotti, M.W.; Mahler, C.F.; Segundo, I.D.B.; Boaventura, R.A.; Vilar, V.J. Development of an integrated treatment strategy for a leather tannery landfill leachate. *Waste Manag.* **2019**, *89*, 114–128. [CrossRef]
156. Changotra, R.; Rajput, H.; Dhir, A. Treatment of real pharmaceutical wastewater using combined approach of Fenton applications and aerobic biological treatment. *J. Photochem. Photobiol. A Chem.* **2019**, *376*, 175–184. [CrossRef]
157. Bener, S.; Atalay, S.; Ersöz, G. The hybrid process with eco-friendly materials for the treatment of the real textile industry wastewater. *Ecol. Eng.* **2020**, *148*. [CrossRef]
158. Giannakis, S.; Gamarra Vives, F.A.; Grandjean, D.; Magnet, A.; de Alencastro, L.F.; Pulgarin, C. Effect of advanced oxidation processes on the micropollutants and the effluent organic matter contained in municipal wastewater previously treated by three different secondary methods. *Water Res.* **2015**, *84*, 295–306. [CrossRef]
159. Ly, Q.V.; Kim, H.C.; Hur, J. Tracking fluorescent dissolved organic matter in hybrid ultrafiltration systems with TiO_2/UV oxidation via EEM-PARAFAC. *J. Membr. Sci.* **2018**, *549*, 275–282. [CrossRef]
160. Piras, F.; Santoro, O.; Pastore, T.; Pio, I.; de Dominicis, E.; Gritti, E.; Caricato, R.; Lionetto, M.G.; Mele, G.; Santoro, D. Controlling micropollutants in tertiary municipal wastewater by O_3/H_2O_2, granular biofiltration and UV254/H_2O_2 for potable reuse applications. *Chemosphere* **2020**, *239*, 124635. [CrossRef]
161. Ponce-Robles, L.; Oller, I.; Polo-López, M.I.; Rivas-Ibáñez, G.; Malato, S. Microbiological evaluation of combined advanced chemical-biological oxidation technologies for the treatment of cork boiling wastewater. *Sci. Total Environ.* **2019**, *687*, 567–576. [CrossRef]
162. De Oliveira Gonçalves, L.; Starling, M.C.V.M.; Leal, C.D.; Oliveira, D.V.M.; Araújo, J.C.; Leão, M.M.D.; Amorim, C.C. Enhanced biodiesel industry wastewater treatment via a hybrid MBBR combined with advanced oxidation processes: Analysis of active microbiota and toxicity removal. *Environ. Sci. Pollut. Res.* **2019**, *26*, 4521–4536. [CrossRef] [PubMed]
163. Rodríguez-Chueca, J.; Amor, C.; Fernandes, J.R.; Tavares, P.B.; Lucas, M.S.; Peres, J.A. Treatment of crystallized-fruit wastewater by UV-A LED photo-Fenton and coagulation-flocculation. *Chemosphere* **2016**, *145*, 351–359. [CrossRef] [PubMed]
164. Amin, M.M.; Golbini Mofrad, M.M.; Pourzamani, H.; Sebaradar, S.M.; Ebrahim, K. Treatment of industrial wastewater contaminated with recalcitrant metal working fluids by the photo-Fenton process as post-treatment for DAF. *J. Ind. Eng. Chem.* **2017**, *45*, 412–420. [CrossRef]
165. Rodríguez-Chueca, J.; Morales, M.; Mosteo, R.; Ormad, M.P.; Ovelleiro, J.L. Inactivation of Enterococcus faecalis, Pseudomonas aeruginosa and Escherichia coli present in treated urban wastewater by coagulation-flocculation and photo-Fenton processes. *Photochem. Photobiol. Sci.* **2013**, *12*, 864–871. [CrossRef] [PubMed]
166. Rodríguez-Chueca, J.; Laski, E.; García-Cañibano, C.; Martín de Vidales, M.J.; Encinas, B.; Kuch, J. Marugán, Micropollutants removal by full-scale UV-C/sulfate radical based Advanced Oxidation Processes. *Sci. Total Environ.* **2018**, *630*, 1216–1225. [CrossRef] [PubMed]